Heliyon 10 (2024) e24710

Contents lists available at ScienceDirect

Heliyon

journal homepage: www.cell.com/heliyon

Research article

Janus kinase inhibitors modify the fatty acid profile of extracellular vesicles and modulate the immune response

Ana María Daza Zapata [a], Karen Álvarez [a], Gloria Vásquez Duque [a], Juliana Palacio [b,c], Mauricio Rojas López [a,d,*]

[a] Grupo de Inmunología Celular e Inmunogenética, Sede de Investigación Universitaria (SIU), Universidad de Antioquia (UDEA), Medellín, Colombia
[b] Grupo De Investigación Ciencia de Los Materiales, Instituto de Química, Facultad de Ciencias Exactas Y Naturales, Universidad de Antioquia (UdeA), Calle 70 No. 52-21, Colombia
[c] Universidad Nacional de Colombia,SedeMedellín, Escuela de Química- Carrera 65 A No 59A-110, Medellín, 4309000, Colombia
[d] Unidad de Citometría de Flujo, Sede de Investigación Universitaria (SIU), Universidad de Antioquia (UDEA), Medellín, Colombia

ARTICLE INFO

Keywords:
Baricitinib
itacitinib
Monocytes
Fatty acids
Platelet aggregation

ABSTRACT

Background: Janus kinase inhibitors (jakinibs) are immunomodulators used for treating malignancies, autoimmune diseases, and immunodeficiencies. However, they induce adverse effects such as thrombosis, lymphocytosis, and neutropenia that could be mediated by extracellular vesicles (EVs). These particles are cell membrane-derived structures that transport cellular and environmental molecules and participate in intercellular communication. Jakinibs can modify the content of EVs and enable them to modulate the activity of different components of the immune response.

Objective: to evaluate the interactions between immune system components of healthy individuals and EVs derived from monocytic and lymphoid lineage cells generated in the presence of baricitinib (BARI) and itacitinib (ITA) and their possible effects.

Methods: EVs were isolated from monocytes (M) and lymphocytes (L) of healthy individuals, as well as from U937 (U) and Jurkat (J) cells exposed to non-cytotoxic concentrations of BARI, ITA, and dimethyl sulfoxide (DMSO; vehicle control). The binding to and engulfment of EVs by peripheral blood leukocytes of healthy individuals were analyzed by flow cytometry using CFSE-stained EVs and anti-CD45-PeCy7 mAb-labeled whole blood. The effect of EVs on respiratory burst, T-cell activation and proliferation, cytokine synthesis, and platelet aggregation was evaluated. Respiratory burst was assessed in PMA-stimulated neutrophils by the dihydrorhodamine (DHR) test and flow cytometry. T-cell activation and proliferation and cytokine production were assessed in CFSE-stained PBMC cultures stimulated with PHA; expression of the T-cell activation markers CD25 and CD69 and T-cell proliferation were analyzed by flow cytometry, and the cytokine levels were quantified in culture supernatants by Luminex assays. Platelet aggregation was analyzed in platelet-rich plasma (PRP) samples by light transmission aggregometry. The EVs' fatty acid (FA) profile was analyzed using methyl ester derivatization followed by gas chromatography.

Results: ITA exposure during the generation of EVs modified the size of the EVs released; however, treatment with DMSO and BARI did not alter the size of EVs generated from U937 and Jurkat cells. Circulating neutrophils, lymphocytes, and monocytes showed a 2-fold greater tendency to

* Corresponding author. Grupo de Inmunología Celular e Inmunogenética, Sede de Investigación Universitaria (SIU), Universidad de Antioquia (UDEA), Medellín, Colombia.
E-mail addresses: mauricio.rojas@udea.edu.co, mrojaslop@hotmail.com (M. Rojas López).

https://doi.org/10.1016/j.heliyon.2024.e24710
Received 27 March 2023; Received in revised form 11 January 2024; Accepted 12 January 2024
Available online 20 January 2024

internalize ITA-U-EVs than their respective DMSO control. The neutrophil respiratory burst was attenuated in greater extent by M-EVs than by L-EVs. Autologous ITA-*M*-EVs reduced T-cell proliferation by decreasing IL-2 levels and CD25 expression independently of CD69. A higher accumulation of pro-inflammatory cytokines was observed in PHA-stimulated PBMC cultures exposed to M-EVs than to L-EVs; this difference may be related to the higher myristate content of M-EVs. Platelet aggregation increased in the presence of ITA-L/M-EVs by a mechanism presumably dependent on the high arachidonic acid content of the vesicles.
Conclusions: Cellular origin and jakinib exposure modify the FA profile of EVs, enabling them, in turn, to modulate neutrophil respiratory burst, T-cell proliferation, and platelet aggregation. The increased T-cell proliferation induced by BARI-L/M-EVs could explain the lymphocytosis observed in patients treated with BARI. The higher proportion of arachidonic acid in the FA content of ITA-L/M-EVs could be related to the thrombosis described in patients treated with ITA. EVs also induced a decrease in the respiratory burst of neutrophils.

List of abbreviations

BARI	Baricitinib
DMSO	Dimethyl sulfoxide
EVs	Extracellular vesicles
ITA	Itacitinib
J	Jurkat cells
L	Lymphocytes
M	Monocytes
U	U937 cells
J-EVs	J-derived EVs
L-EVs	L-derived EVs
M-EVs	Monocyte-derived EVs
U-EVs	U-derived-EVs
RPMI	Roswell Park Memorial Institute Medium
BARI-J-EVs	J-EVs released under BARI exposure
BARI-L-EVs	L-EVs released under BARI exposure
BARI-*M*-EVs	M-EVs released under BARI exposure
BARI-U-EVs	U-EVs released under BARI exposure
DMSO-J-EVs	J-EVs released under DMSO exposure
DMSO L-EVs	L-EVs released under DMSO exposure
DMSO-*M*-EVs	M-EVs released under DMSO exposure
DMSO-U-EVs	U-EVs released under DMSO exposure
ITA-J-EVs	J-EVs released under ITA exposure
ITA-L-EVs	L-EVs released under ITA exposure
ITA-*M*-EVs	M-EVs released under ITA exposure
ITA-U-EVs	U-EVs released under ITA exposure
CFSE	Carboxyfluorescein Succinimidyl Ester
DHR123	Dihydrorhodamine 123
DLS	Dynamic Light Scattering
iFBS	Heat-inactivated Fetal Bovine Serum
PDI	Polydispersity Index
PI	Propidium Iodide
PRP	Platelet Rich Plasma
TEM	Transmission Electron Microscopy
DVT	Deep Vein Thrombosis
PE	Pulmonary Embolism
RA	Rheumatoid Arthritis
VTE	Venous thrombo-embolism

1. Introduction

JAKs and STATs are proteins involved in intracellular signaling and regulation of genes involved in cells growth and differentiation

as well as inflammation-related genes [1,2]. JAK-STAT anomalies are linked to disorders such as myeloproliferative diseases and lymphomas. Also, the expression of SOCS1, a JAK-STAT pathway repressor, is reduced in patients with systemic lupus erythematosus (SLE) [3]. JAK inhibitors (jakinibs) have been developed for treating cancer [4,5] and curbing inflammation [6] and autoimmune responses [7–9].

Tofacitinib and baricitinib (**BARI**) are U.S. Food and Drug Administration (FDA)-approved jakinibs considered safe for treating patients with rheumatoid arthritis (RA). Upon treatment with these jakinibs, patients with RA showed less fatigue and a 50 % decrease in joint pain [10,11]. In addition, jakinibs also decrease TNF-α accumulation and interferon-gamma (IFN-γ)-associated gene expression [7,12–14].

BARI has been successful in patients with RA, but it has been reported to cause neutropenia and lymphocytosis [15–17]. Less than ten percent of the RA patients treated with BARI had neutropenia with a count of less than 1500 neutrophils/mm^3 [15,18], and 90 % of patients with RA have a non-significant decrease in the neutrophil count [17]. Fifteen percent of patients with SLE treated with **BARI** showed absolute neutrophil counts below 2000 cells/mm^3 [19]. Furthermore, lymphocytosis was observed after one week of BARI treatment in patients with psoriasis (20 % increase up to week 4) [20], RA (significant increase of 30 % up to week 12) [15,16], and SLE (non-significant increase up to week 24; appendices) [19].

Itacitinib (ITA), a selective JAK1 inhibitor [21], not yet approved by the FDA, has been used in some trials to treat patients with myelofibrosis, breast adenocarcinoma, and acute graft-versus-host disease (aGVHD). However, long-term ITA treatment has been reported to induce neutropenia [22–25]. Patients with myelofibrosis and adenocarcinoma treated with ITA showed neutropenia with a count of less than 1000 neutrophils/mm^3 [22,23]. Likewise, neutropenia was observed in 45 % of patients with aGVHD under ITA treatment [25].

The precise mechanism responsible for jakinib-induced thrombosis is far from clear. Jakinibs may indirectly affect the FA content of leukocyte membranes by modulating signaling pathways involved in their metabolism or events of the immune response [26]. The FA oxidation can fuel agonist-induced platelet activation and thrombus formation [27]. In addition, the JAK2-STAT3 pathway is involved in collagen-induced platelet activation [28]. Moreover, the JAK2-JNK/PKC-STAT3 signaling pathway is also implicated in this process [29]. These findings suggest that jakinibs could potentially modulate platelet activation.

Extracellular vesicles are particles naturally released by cells and enclosed within a lipid bilayer [30]. These vesicles can be considered indicators of an organism's homeostasis. In addition, they serve as intercellular communicators due to their varied content and many interactions with cells [31–33]. Since EVs can induce respiratory burst, platelet aggregation, and T-cell proliferation, they may contribute to neutropenia, cardiac events, and lymphocytosis.

Extracellular vesicles have diverse effects, such as induction of neutropenia through increased respiratory burst, and may be key players in anti-inflammatory processes. Their impact on reactive oxygen species (ROS) accumulation varies depending on their cellular origin, types of target cells, and cellular environment [34]. For example, NADPH oxidase-rich EVs derived from aortic endothelial cells of C57BL6/J mice promoted cellular accumulation of ROS [35], and EVs released from pancreatic tumor cells induced ROS production by human monocytes [36].

Depending on their cellular origin, EVs can stimulate or inhibit T-cell proliferation [37–40]. For example, CD4+FasL + T cells-derived EVs loaded with ovalbumin can suppress naïve T-cell proliferation by inducing lymphocyte death through FasL-CD95 interactions. Conversely, EVs released by U937 cells, dendritic cells, and human monocyte-derived macrophages enhanced allor-eactive T-cell proliferation by expressing the surface co-stimulatory molecules CD80, CD86, and HLA-DR.

Extracellular vesicles released by circulating cellular elements have been associated with platelet aggregation and coagulation [41]. Indeed, EVs can be rich in lipids such as phosphatidylserine [42] and arachidonate [43] and enzymes such as secretory phos-pholipase A2 [44], all of which are involved in thrombus formation [45]. In addition, EVs may contain proteins of the coagulation cascade, such as factors X, VII, and III (tissue factor) [46]. These lipids and proteins could be related to the cardiovascular disorders described in patients undergoing therapy with jakinibs. Of note, platelet-derived EVs may exert an anticoagulant effect by inactivating factor Va [41].

We hypothesized that some of the adverse effects associated with therapies with jakinibs are mediated by EVs released under treatment with these drugs. This work evaluated the composition of EVs derived from human lymphoid and monocytic lineage cells exposed *in vitro* to BARI and ITA and their effects on human circulating leukocytes and platelets. The lipid composition of EVs varied depending on the cell source and the jakinib used. Furthermore, when co-incubated with neutrophils, lymphocytes, monocytes, and platelets, the EVs modulated neutrophil respiratory burst, T-cell proliferation, and platelet aggregation.

2. Materials and methods

2.1. Reagents, materials, and antibodies

RPMI-1640 medium, Dulbecco's phosphate buffered saline (DPBS), fetal bovine serum (FBS), Histopaque-1077, penicillin (5000 IU)-Streptomycin (5 μg), trypan blue dye, anhydrous dimethyl sulfoxide (DMSO ≥99.9 %), Phorbol myristate acetate (PMA), and phytohemagglutinin A (PHA) derived from *Phaseolus vulgaris* were purchased from Sigma-Aldrich (St. Louis, MO, USA). RNase A (DNase and protease-free) and Igepal™ CA-630 were purchased from Thermo Fisher Scientific, Inc. (Pittsburgh, PA, USA). Ethyl-enediaminetetraacetic acid (EDTA) was obtained from Promega (Madison, WI, USA). Propidium Iodide (PI), Annexin-V, Annexin-V binding buffer, Cytofix™ fixation buffer, Phosflow™ wash, and permeabilization buffer, Pharmingen™ stain, and FACSFlow™, were purchased from BD Pharmingen (San Diego, CA, USA). AG126 and AG490 inhibitors were obtained from Calbiochem (San Diego, CA, USA). Jakinibs (itacitinib and baricitinib) were purchased from Cayman Chemical (Ann Arbor, MI, USA). Carboxyfluorescein

succinimidyl ester (CFSE), dihydrorhodamine 123 (DHR123), and Life/death cell viability Vioblue, and 3,3′-dihexyloxacarbocyanine iodide ($DIOC_6$) dyes were purchased from Thermo Fisher Scientific, Inc. (Pittsburgh, PA, USA). ELISA kit for quantifying Arachidonic Acid (Abcam, Cambridge, UK; detection range = 78.125 ng/mL – 5000 ng/mL)

Vacutainer®EDTA and Vacutainer®citrate blood collection tubes, were purchased from BD Pharmingen. Polyethylene tubes (12 mm × 75 mm) were purchased from BD Falcon (San Diego, CA, USA). Acrodiscs® syringe filters with 0.2 - μm membrane were purchased from Advantec (Tokyo, Japan). Cell culture 48- and 96-well plates were obtained from Corning (New York, NY, USA). Sphero™ polystyrene beads (NFPPS-015-5; 220 nm to 1.3 μm in size) (were purchased from Sperothech (Lake Forest, IL, USA).

Fluorochrome-conjugated anti-human mAbs used for flow cytometry (FCM) analysis were: CD14-RD1, (clone MY4, 322 A-1) from Beckman Coulter; CD56-PE (clone B159), CD19-V450 (clone HIB19), CD3-PeCy7 (clone UCHT-1), CD45-PeCy7 (clone 30-F11), CD8-PeCy5 (clone HIT8A), CD25-PeCy5 (clone M-A251), CD69-PE (clone FN50), and Stat1 (pY701)-Alexa Fluor®647 (clone 4a) (RUO) from BD Biosciences (San Diego, CA, USA); HLA-DR-APCCy7 (clone L243) from Biolegend (San Diego, CA, USA); HMGB1-APC (clone 115603) from R&D systems (Minneapolis, MN, USA); and CD3-E Fluor 450 (clone 17A2) from Thermo Fisher Scientific, Inc.

2.2. Isolation of peripheral blood mononuclear cells

Peripheral blood samples were collected from 26 healthy volunteers (7 women and 19 men) aged between 20 and 30 years. Blood samples were drawn into Vacutainer® EDTA tubes (for *in vitro* cell cultures) and onto glass beads for defibrination (for monocyte enrichment by adherence to plastic and subsequent isolation of EVs). Both samples were diluted 1:1 with DPBS and centrifuged on a density gradient using Histopaque (1077 g/L) at 900×*g* for 30 min at room temperature (RT); then, peripheral blood mononuclear cells (PBMCs) were removed and washed with DPBS. Cell number and viability were determined by trypan blue dye exclusion using a Neubauer chamber (viability was always ≥98 %). In addition, PBMCs isolated from defibrinated blood samples were stained with anti-CD14-RD1 conjugated mAb and acquired on LSRFortessa™ cell flow cytometer (BD Biosciences) to calculate the $CD14^+$ monocyte concentration.

PBMCs were then resuspended in RPMI 1640 medium without antibiotics and supplemented with heat-inactivated FBS (56 °C for 40 min) (iFBS).

2.3. 2.3sorting of lymphocytes and monocytes

A total of 10×10^6 PBMCs were resuspended in 1 mL of RPMI with 2 % EDTA. They were then labeled with anti-CD3-PE-Cy7 and anti-CD14-RD1 conjugated mAbs for two-way sorting using the BD FACSAria™III Cell Sorter (BD Biosciences). Cells were collected in RPMI 1640 supplemented with 4 % iFBS.

2.4. Monocyte enrichment by adherence to plastic plates

PBMC suspensions (containing 3×10^5 $CD14^+$ cells) were seeded per well in 48-well polystyrene tissue culture plates and resuspended in 500 μL of RPMI 1640 supplemented with 0.5 % v/v iFBS. Cells were incubated at 37 °C in a 5 % CO_2 atmosphere for 2 h, and then washed with DPBS containing 0.5 % iFBS to remove non-adherent cells. Cells adhered to the plate were incubated in 500 μL of RPMI supplemented with 10 % iFBS at 37 °C and 5 % CO_2. After 24 h, cells were detached with a glass scrapper and suspended in RPMI supplemented with 10 % iFBS. To verify monocyte enrichment and determine their purity, cells were stained with anti-CD19-V450, anti-CD3-PE-Cy7, and anti-CD56-PE mAbs and acquired on a BD LSRFortessa™ cell flow cytometer [47].

2.5. Inhibitory activity of non-cytotoxic concentrations of jakinibs

The inhibition of the JAK-STAT pathway by the non-cytotoxic concentrations of jakinibs chosen for the present experiments according to previously published data was evaluated in terms of STAT1 phosphorylation at Y701. For this purpose, monocytes detached from polystyrene plates (300.000 cells/500 μL RPMI 10 % iFBS), were exposed for 1 h to reported non-cytotoxic concentrations of ITA (25 μM), BARI (200 nM), the JAK2 inhibitor AG490 (25 μM), and the tyrosine kinase inhibitor AG126 (12.5 μM); 0.5 % DMSO was used as a vehicle control. Cells were then stimulated with 2 ng/mL IFN-γ for 10 min, fixed, permeabilized, and stained with anti-STAT1 (pY701)-Alexa Fluor 647, according to the BD™PhosphoFlow protocol [48], and acquired on the BD LSRFortessa™ cell flow cytometer.

2.6. HLA-DR expression on jakinib-treated monocytes

The effect of jakinibs on IFN-γ-induced HLA-DR expression in peripheral blood monocytes was also evaluated. For this purpose, 3×10^5 PBMCs/well were seeded in 48-well cell culture plates and resuspended in 500 μl RPMI 1640 supplemented with 10 % iSBF, exposed to jakinibs and controls (at concentrations described above), for 1 h and stimulated with 2 ng/mL IFN-γ. After 24 h, cells were stained with Propidium iodide (PI) (to exclude dead cells), anti-HLA-DR-APCCy7, anti-CD19-V450, and anti-CD14-RD1 mAbs and acquired on the BD LSRFortessa™ cell flow cytometer.

2.7. Isolation of EVs from in vitro cell cultures exposed to jakinibs

Extracellular vesicles were isolated from sorted lymphocytes, sorted monocytes, as well as from lymphoblastoid Jurkat (ATCC TIB-152) and promonocytic U937 (ATCCCRL-1593) cell lines exposed to jakinibs as follows.

Sorted lymphocytes and monocytes, were seeded into 48-well cell culture plates (3×10^5 cells per well in 500 μL of RPMI medium supplemented with 10 % iFBS previously filtered through 0.2 μm-pore size nylon membrane). Next, cells were treated for 24 h with a combination of 25 μM ITA and 200 nM BARI. DMSO (0.5 %) was used as vehicle control. ITA and BARI concentrations were determined from results of the viability assays (data not shown).

Additionally, the $CD4^+$ lymphoblastoid Jurkat and the promonocytic U937 cells (2.5×10^5) were cultured in 25 cm^2 tissue culture flasks containing 5 mL of RPMI medium supplemented with 1 % streptomycin-penicillin and 10 % filtered iFBS, 25 μM ITA, 200 nM BARI, and 0.5 % DMSO (vehicle control). After 24 h, cell viability and cell cycle were assessed (data not shown), and EVs were isolated as follows.

Cells were centrifuged at 600×*g* for 10 min. Culture supernatants were collected in 1.5 mL Eppendorf® tubes and centrifuged at 17,000×*g* for 1 h to pellet EVs [49]. Supernatants were discarded, leaving the pellets (containing the EVs) resuspended in 100 μL of the culture medium. Afterward, EVs were washed with 1 mL of filtered RPMI followed by centrifugation at 17,000×*g* for 1 h to remove traces of inhibitors. The supernatants were discarded, leaving EVs pellets resuspended in 100 μL of medium. Finally, 100 μl of filtered DPBS were added and the EV suspensions were frozen at −70 °C.

2.8. Characterization of EVs generated in vitro

2.8.1. Dynamic light scattering: The size and size distribution of the EVs isolated were determined on a Horiba LB 550 dynamic light scattering (DLS) system (Minami-ku, Kyoto, Japan) in an aqueous medium at neutral pH and RT. The hydrodynamic diameters of the particles were calculated using the Stokes-Einstein equation. All measurements were performed five times. The size of EVs was reported as mean hydrodynamic diameter ± Standard deviation (SD). The polydispersity index (PDI) was calculated as the square of the standard deviation divided by the square of the mean $(SD/mean)^2$.

2.8.2. Transmission electron microscopy (TEM): Representative samples of EVs were evaluated by TEM. Briefly, vesicles were washed with 0.5 X DPBS, applied to copper-coated carbon grids, and dried on racks at 40 °C. Negative staining was also performed for better visualization of EVs by pre-treatment with 2 % w/v uranyl acetate solution and drying at RT. Vesicle preparations were visualized on a Tecnai™G^2 F20 TE microscope (FEI Company, Hillsboro, OR, USA); EVs images were captured with an UltraScan®1000XP camera (Gatan, Inc, Pleasanton, CA, USA).

2.9. Internalization of EVs by peripheral blood leukocytes

Frozen suspensions of EVs (200 μL) were brought to a volume of 1 mL with filtered DPBS, stained with 0.5 μl of CFSE (5 μM), and incubated for 10 min at 37 °C. Then, 100 μl of filtered iFBS were added and the incubation was prolonged for another 5 min. Afterward, EVs were centrifuged at 17,000×*g* for 1 h, and the supernatants were discarded. Then, to remove the excess CFSE dye, EVs were incubated with 1 mL of RPMI supplemented with 10 % filtered iFBS for 40 min, and then centrifuged at 17,000×*g* for 1 h. A 10 μl aliquot of the CFSE-stained EVs was used for direct counting on the CytoFLEX flow cytometer (Beckman Coulter, Brea, CA, USA).

EDTA-anticoagulated peripheral blood (25 μL) from healthy volunteers was diluted with 300 μl of RPMI in 12 × 75 mm polyethylene tubes and incubated for 1 h with different concentrations of CFSE-stained EVs (0.75×10^6, 2.25×10^6 and 3.75×10^6). Anti-CD45-PeCy7 was then added to stain the leukocytes. Events were acquired on the BD LSRFortessa™ flow cytometer by setting a threshold based on the FSC-H and CD45-PeCy7 fluorescence signals. A first acquisition was performed to assess the percentage of cells bound to EVs or that had internalized EVs. Subsequently, leukocyte fluorescence corresponding to membrane-bound EVs was quenched by adding trypan blue at a final concentration of 0.3 % v/v [50]. A second acquisition was then performed to assess only the percentage of leukocytes that had ingested EVs.

2.10. Neutrophil isolation and ROS production

Neutrophils were isolated through density gradients following the protocol of Kuhns et al. [51]. Briefly, neutrophils (2×10^5 cells/300 μL) were deposited into 12 mm × 75 mm polyethylene tubes containing RPMI 1640 and stained with DHR123, at a final concentration of 5 nM, and incubated at 37 °C in a water bath for 10 min. Subsequently, cells were exposed to 1.75×10^6 L-EVs and M-EVs for 40 m at 37 °C. After incubation, neutrophils were stimulated with PMA, at a final concentration of 10 ng/mL, for 10 min. Cells were acquired on a BD LSRFortessa™ cell flow cytometer [52].

2.11. T-cell activation and proliferation

PBMCs were stained with 1 μL of CFSE (5 μM) in 10 mL of PBS and incubated for 20 min at 37 °C and 5 % CO_2. Subsequently, they were centrifuged at 600×*g* for 10 min, and the supernatant was removed. Next, cells were incubated with RPMI supplemented with 10 % iFBS for 40 m at 37 °C and 5 % CO_2 to eliminate the excess CFSE dye. CFSE-stained PBMCs (1×10^5 cells per well in 200 μl of RPMI 1640 supplemented with 5 % v/v iFBS) were then seeded in 96-well cell culture plates. Cell proliferation was induced with 4 % v/v PHA (0.1 mg/mL) in the presence of 1.25×10^6 L-EVs and M-EVs released under treatment with jakinibs. After 6 h of PHA stimulation,

supernatants were collected to quantify cytokines, and incubation went on to complete 96 h at 37 °C and 5 % CO_2. Cells were finally stained with Life/Death-Violblue to exclude dead cells and were labeled with fluorescent anti-CD69-PE, anti-CD25-Pe-Cy5, anti-CD8-PeCy5, and anti-CD3-PeCy7 mAbs. Cells were acquired on a BD LSRFortessa™ cell flow cytometer.

2.12. Quantification of cytokines

The levels of IL-2, MIP-1α, MIP-1β, IP-10, IL-1β, RANTES, IL-4, MCP-1, VEGF, IL-17, IL-10, IL-1Rα, IL-8, and TNF-α in cell culture supernatants were quantified by flow cytometry using the Luminex® 200™ system and the xPONENT® software following the manufacturer's instructions.

2.13. Platelet aggregation

Citrate-anticoagulated peripheral blood samples drawn from healthy individuals were centrifuged at 1800×*g* for 140 min to obtain platelet-rich plasma (PRP). PRP samples (50 μL) were mixed with EV suspensions (30 μL) in cuvettes maintained at 37 °C and stirred at 600 rpm in a Lumi-Aggregometer PAP-8E (Sentinel Diagnostics, MI, Italy); measurements were recorded every 8 min.

2.14. Analysis of fatty acids

2.14.1. Fatty acid extraction

The isolated EVs were resuspended in 1.7 mL of $CHCl_3$:CH_3OH (2:1 v/v) and vortexed vigorously for 2 min. Then, 0.650 mL of $CHCl_3$ were added, followed by vortexing for 1 min. Subsequently, 650 μL of 0.8 % (w/v) KCl in saline was added followed by vortexing for 1 min. The samples were centrifuged at 1800×*g* for 5 min at 4 °C to collect the organic phase; this procedure was repeated once more. The collected organic phases were mixed, and frozen at −20 °C until derivatization [53].

2.14.2. Fatty acid methyl ester derivatization

Samples containing FAs were dried under nitrogen and methylated as described elsewhere [54]. Briefly, the carboxylic acids were esterified as follows: MeOH/NaOH refluxed at 90 °C for 7 min, boron trifluoride CH_3OH (catalyst) refluxed for 2 min, heptane (1 mL) refluxed for 1 min, followed by washing with saturated NaCl solution and extraction of the product in heptane into glass stoppered vials. Finally, samples containing the fatty acid methyl esters (FAMEs) were loaded on the gas chromatograph system (Agilent; Santa Clara, CA, USA) for analysis.

2.14.3. Gas chromatography. Standard addition method

Two microliters of each sample were mixed with internal standards (C19 or AA) and injected into the gas chromatograph. A FAME column (FAMEs model jiwdb23; Agilent) and hydrogen gas were used. Chromatographic conditions were as follows: Inlet gas flow rate of 40 mL/min; injector temperature of 220 °C, detector temperature of 240 °C, and column pressure of 23.04 psi. A split injection was carried out without automated sampling, and the temperature ramp for FAMEs separation comprised an initial column temperature of 200 °C for 10 min which was then increased at a rate of 20 °C/min to 220 °C.

2.14.4. Arachidonic acid quantification

Culture media samples and EV-derived lysates obtained after thawing were centrifuged at 20,000×*g* for 10 min at 4 °C. Then, supernatants were collected for AA quantification using an ELISA KIT (Abcam, Cambridge, UK), following the manufacturer's instructions. The kit was supplied with anti-AA-biotin mAb, streptavidin-HRP conjugate, H_2O_2/tetramethylbenzidine (TMBS), and acid to stop the enzymatic reaction. Abs450nm was determined in a spectrophotometer (Multiskan SkyHigh Microplate Spectrophotometer (Thermo Fisher Scientific Inc., Waltham, MA) immediately after incubation at 37 °C for 10 min. Each sample was analyzed in triplicate.

2.15. Experimental design and statistics

Experimental design. First, the doses of jakinibs to be used in the experimental assays were optimized according to their effects on the surface HLA-DR expression and STAT-1 phosphorylation in IFN-γ-stimulated monocytes. Next, U937 (myeloid) and Jurkat (lymphoid) cells were used as a primary source of EVs. Additionally, for comparison with primary cells, EVs were isolated from $CD3^+$ T cells and $CD14^+$ monocytes electromagnetically sorted and exposed to optimized doses of jakinibs. All these EVs were then characterized by DLS, TEM, FA content by GC-FAME, and flow cytometry (Supplementary Figure S1). Once identified as EVs, the isolated vesicles were labeled with CFSE and co-incubated with human peripheral blood to study their uptake by different leukocyte subsets. Subsequently, the effects of EVs on neutrophil (ROS production), T cells (activation, proliferation, and cytokine synthesis), and platelets (aggregation) were evaluated. Finally, the significant effects exerted by EVs were confirmed in assays with isolated lymphocytes or monocytes to define activities associated explicitly with myeloid or lymphoid cell populations.

Statistics. The sample size was calculated based on previously published data [55]. Normality and homogeneity of variances were determined for each set of experiments. All experimental data failed the Shapiro-Wilk test for normality. Therefore, Kruskal-Wallis one-way ANOVA or two-way ANOVA was used to determine significant differences between independent groups. Dunn's and Bonferroni's tests were applied as post hoc tests for multiple comparisons. The Wilcoxon test was run to compare paired data. Statistical significance was set at critical values of $*p \leq 0.05$, $**p \leq 0.01$, and $***p \leq 0.001$. Analyses were run on GraphPad Prism version 8.0

(GraphPad Software Inc., San Diego, CA, USA) and STATGRAPHICS Centurion XVI, version 16.1.18 (Statistical Graphics Corporation, Rockville, MD, USA) software. Flow cytometry data were analyzed using the FlowJo™ version 10.1. software (BD Life Science, Ashland, OR, USA).

3. RESULTS

3.1. Non-cytotoxic concentrations of jakinibs inhibited IFN-γ-induced STAT1 activation

We selected the minimum non-cytotoxic concentrations of jakinibs and control inhibitors (AG126 and AG490) according to PBMC viability data published in the literature [56–58], as follows: 200 nM for BARI, 12.5 μM for AG126, and 25 μM for AG490 and ITA. PBMCs exposed to these doses of inhibitors for 24 h showed more than 70 % of DIOC6^{high} cells and less than 20 % DIOC6^{low} cells (Supplementary Fig. S2) [56–58].

Then, the impact of non-cytotoxic doses of jakinibs on STAT1 phosphorylation (pY701) in IFN-γ-stimulated monocytes was analyzed. This assay was intended to assess whether the selected doses of jakinibs could altered the STAT1 signaling pathway as expected, and the generation of EVs. Plastic adherent monocytes were pre-treated with 200 nM BARI and 25 μM ITA for 1 h before IFN-γ stimulation. STAT1 (pY701) was not diminished in the presence of AG126 or AG490 (Fig. 1A and B), but it was significantly reduced in monocytes exposed to either jakinib (Fig. 1C, D and E, *p < 0.05).

The up-regulation of the HLA-DR expression in response to IFN-γ depends on the JAK-STAT1 signaling pathway and is a well-known phenomenon. In the present study, the activity of the selected doses of jakinibs was also evaluated by analyzing the HLA-DR expression on peripheral blood monocytes stimulated with IFN-γ. In Fig. 2A, the gating strategy is depicted for delineating HLA-DR expression on viable (PI-), single monocytes (CD14^{+}). The HLA-DR expression on monocytes exposed to DMSO was significantly decreased in the presence of ITA ($p < 0.01$), AG126 ($p < 0.001$), and AG490 ($p < 0.05$), regardless of IFN-γ stimulation. However, this effect was not observed in the presence of BARI (Fig. 2B). Cell viability after experimental interventions exceeded 95 % in all cases (Fig. 2C). In conclusion, low, non-cytotoxic concentrations of ITA and BARI effectively inhibit the JAK-STAT1 signaling pathway in IFN-γ-stimulated monocytes isolated from peripheral blood.

3.2. U937 and Jurkat cells treated with jakinibs released heterogeneous-sized EVs

To address the challenge of limited EV recovery from peripheral blood monocytes (EV-M) and lymphocytes (EV-L) and for optimizing the control of the experimental setting, U937 and Jurkat cells were selected as alternative sources of EVs. These cell lines were

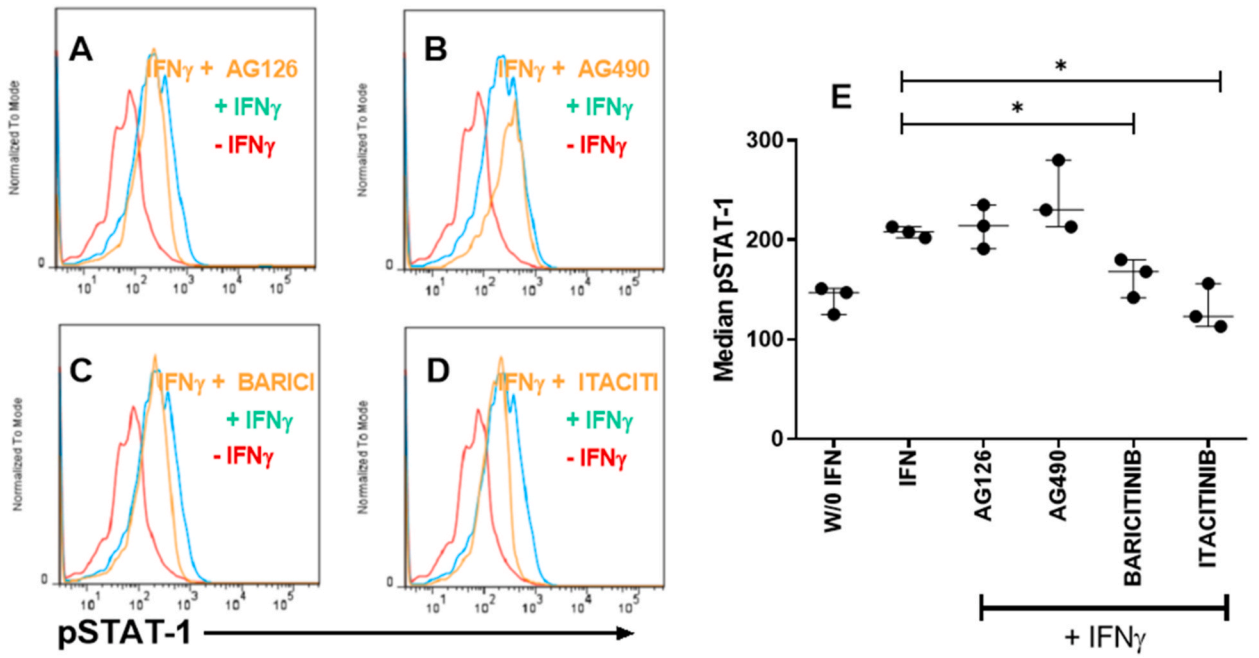

Fig. 1. Inhibition of STAT1 phosphorylation in monocytes by non-cytotoxic concentrations of jakinibs. Monocytes isolated by adherence to plastic were pre-treated with 12.5 μM AG126 (**A**), 25 μM AG490 (**B**), 200 nM bariticinib (**C**), and 25 μM itacitinib (**D**) for 1 h and then stimulated with IFN-γ for 10 min. STAT1 phosphorylation was assessed by flow cytometry using anti-STAT1 (pY701)-Alexa Fluor®647 mAb. $p < 0.05$; **$p < 0.01$; ***$p < 0.001$ correspond to differences when compared to IFN-γ-stimulated cells (**E**). Representative histograms of one experiment. The dot plot chart shows the median MFI ± IQR of STAT1 (pY701). n = 3 independent experiments.

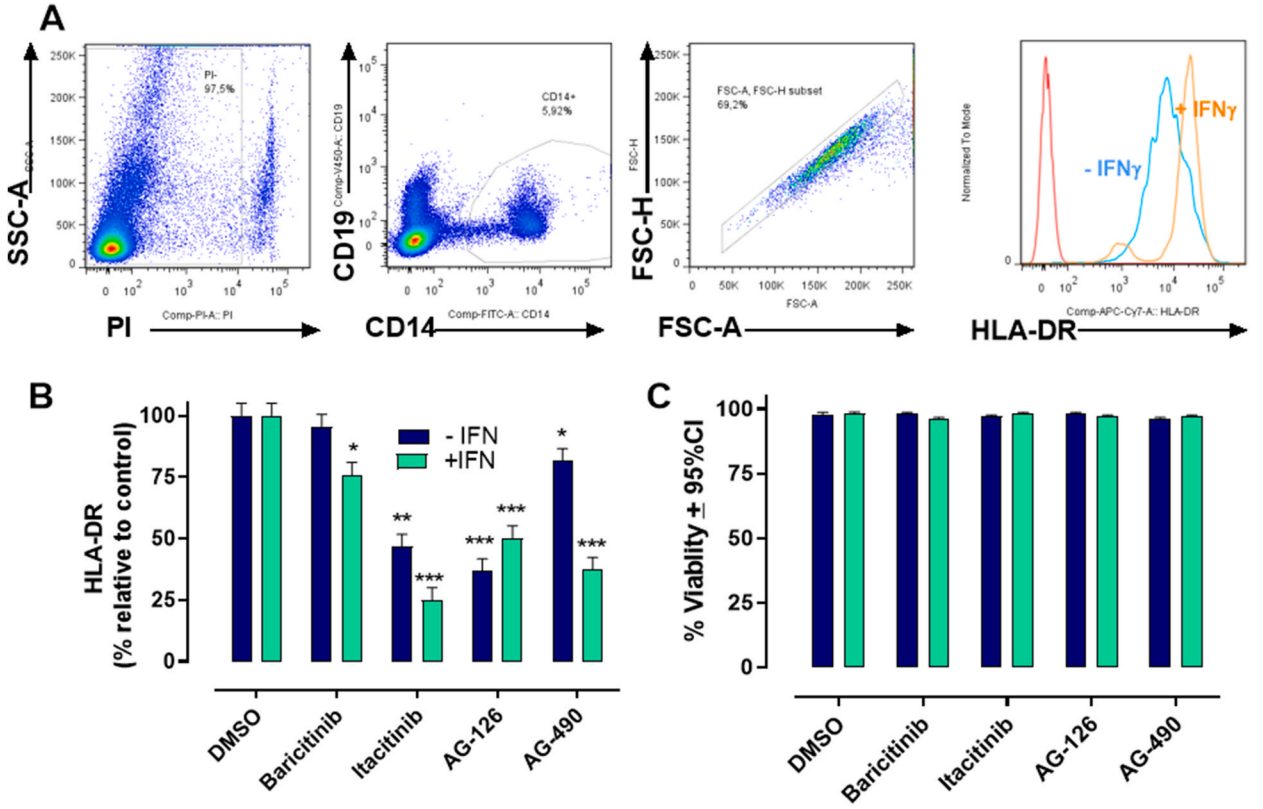

Fig. 2. Inhibition of HLA-DR expression on monocytes by non-cytotoxic concentrations of jakinibs. Human PBMCs were pre-treated with 200 nM baricitinib, 12.5 μM AG126, 25 μM AG490 and 25 μM itacitinib for 1 h, and then stimulated with IFN-γ for 24 h. Cells were stained with PI, anti-HLA-DR-APC-CY7, anti-CD19-V450, and anti-CD14-RD1 mAbs. **A.** Gating strategy for $CD14^+$ cells (monocytes), and representative histograms of HLA-DR expression in monocytes cultured with and without IFN-γ. **B.** The bar chart represents the mean % ± 95%CI of HLA-DR MFI on monocytes relative to HLA-DR MIF in DMSO controls. Overton subtractions were performed to evaluate differences between treatments **C.** The bar chart represents the mean % ± SEM of cell viability relative to DMSO controls after 24 h-incubation with or without IFN-γ evaluated by PI exclusion and flow cytometry. *$p < 0.05$; **$p < 0.01$; ***$p < 0.001$ differences when compared to control without IFN-γ. Two-way ANOVA and post hoc Bonferroni's tests n = 3 independent experiments.

also valuable controls to define whether the release of EVs in the presence of jakinibs could be attributed to the inhibitors themselves or whether it was a phenomenon inherent to the cell source.

To ensure that EVs released from jakinib-treated U937 cells (BARI-U-EVs and ITA-U-EVs) and jakinib-treated Jurkat cells (BARI-J-EVs and ITA-J-EVs) did not come from apoptotic bodies, cell viability and apoptosis were evaluated. U937 and Jurkat cells were exposed to ITA, BARI, and DMSO (vehicle control) for 24 h, stained with PI, and analyzed by. flow cytometry (data not shown). Cell viability remained consistently above 95 %, and no evidence of DNA fragmentation was observed.

The isolated EVs were characterized by different methods. First, DLS measurements were used to calculate the size and PDI of U-EVs and J-EVs. The size of both types of vesicles showed a normal distribution but varied as a function of the jakinib treatment. ITA-J-EVs (mean diameter = 455 ± 111 nm; PDI = 0.06) were smaller than J-EVs released in the presence of DMSO (DMSO-J-EVs) and BARI (BARI-J-EVs) (mean diameter = 583 ± 137 nm; PDI = 0.05) (Fig. 3A). The calculated PDI values (less than 0.1) indicated that all the EVs isolated had a narrow unimodal size distribution.

On the other hand, EVs released from U937 cells cultured in RPMI exposed to DMSO or BARI showed a bimodal size distribution. U-EVs derived from cell cultures exposed to DMSO or BARI included small particles with mean diameters of 444 ± 180 nm and 425 ± 170 nm, respectively, and large particles with mean diameters of 1976 ± 719 nm and 2105 ± 742 nm, respectively. Interestingly, ITA treatment induced U-EVs with a unimodal size distribution (821 ± 543 nm; PDI = 0.44) (Fig. 3B). The size of all isolated EVs populations was corroborated by TEM (Fig. 3C).

3.3. Jakinibs do not alter protein expression on the surface of EVs

Janus kinase-dependent signaling pathways are known to modulate the surface expression of several cellular receptors. Therefore, cells exposed to jakinibs are expected to release EVs phenotypically different from those generated from cells not exposed to any treatment.

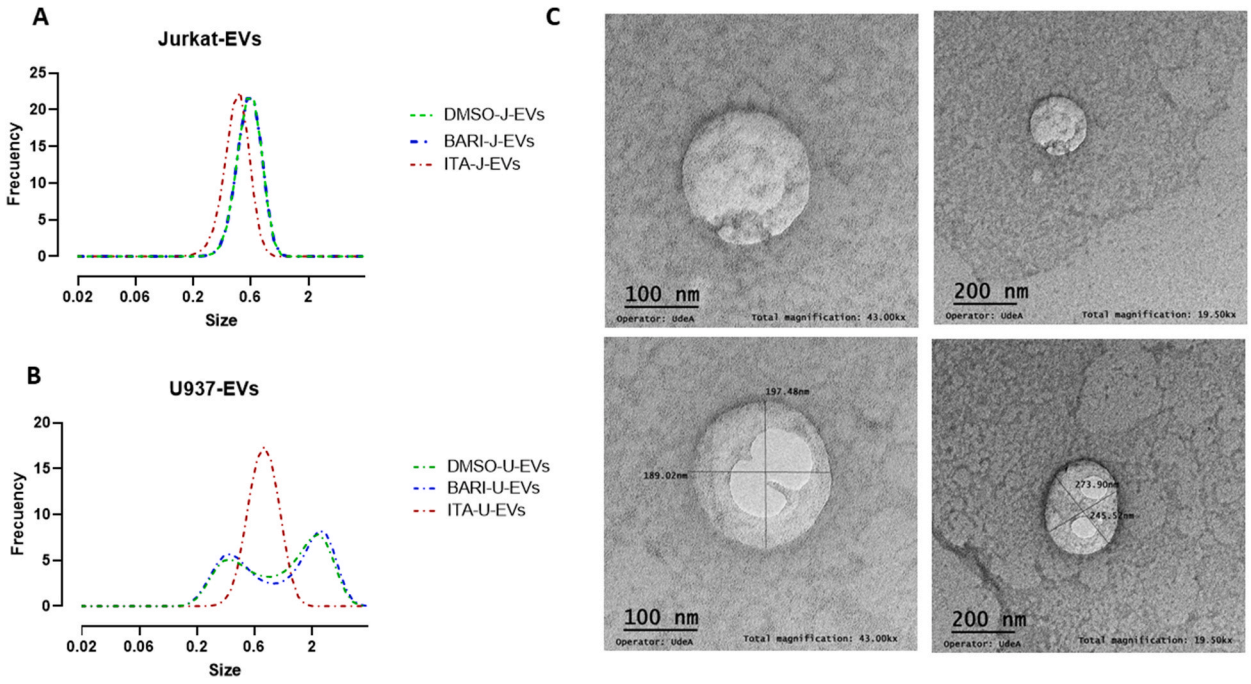

Fig. 3. Size of extracellular vesicles derived from Jurkat and U937 cells treated with jakinibs. Extracellular vesicles were isolated from Jurkat **(A)** and U937 **(B)** cells cultured in the presence of 200 nM baricitinib (BARI), 25 μM itacitinib (ITA), or 0.5 % DMSO (vehicle control) for 24 h. The absolute sizes of EVs were determined by dynamic light scattering. **C.** EVs were negatively stained and analyzed under TEM. Images captured by UltraScan ®1000XP camera. Particle diameters are shown; n = 1 independent experiment.

Cytometry analyses showed that the surface expression of $CD45^+$, $CD4^+$, $CD3^+$, $CD14^+$, and HLA-DR were similar in EVs isolated from all sources. Moreover, the presence of HMGB1 on the vesicle surface and the exposure of phosphatidylserine on the outer leaflet of the vesicle membrane were evaluated by labeling with anti-HMGB1-APC mAb and Annexin V, respectively, and flow cytometry. These surface markers were evaluated for their involvement in the immunogenicity of EVs and their potential as biomarkers to monitor treatment outcomes. HMGB1 was not detected in any group of EVs. Supplementary Fig. S3 shows those ones isolated from primary cells.

3.4. ITA-U-EVS were mainly ingested by circulating phagocytes

Since EVs can target different target cells and induce diverse effects on them, the interaction between EVs and peripheral blood leukocytes was assessed. The binding and uptake of EVs by circulating leukocytes were evaluated by flow cytometry after incubating CD45-PeCy7-labeled-blood samples with increasing concentrations of CFSE-labeled EVs released from Jurkat and U937 cells previously exposed to DMSO, ITA, and BARI. CFSE + leukocytes corresponded to those that could bind or internalize EVs. After the addition of trypan blue to quench CFSE fluorescence on the leukocyte membrane, fluorescent signals corresponded only to internalized EVs.

A dose-dependent effect was evident in the internalization of J-EVs and U-EVs by neutrophils (Fig. 4A), lymphocytes, and monocytes (data not shown). It is noteworthy that EVs binding was a saturable process; therefore, the proportion of cells able to internalize EVs at the two highest concentrations of EVs were very similar.

Supplementary Figs. S4A and S4B show the consolidated percentages of leukocytes that internalized J-EVs and U-EVs released from cell cultures exposed to DMSO, ITA, and BARI. When blood samples were incubated with 3.75×10^6 EVs, 60 % of neutrophils, 50 % of monocytes, and 10 % of lymphocytes were observed to internalize vesicles regardless of their cellular origin. Thus, the cellular source of EVs did not affect the ability of circulating leukocytes to internalize them.

The effect of jakinibs on EV uptake by leukocytes was assessed in cultures of blood samples co-incubated with 0.75×10^6 J-EVs and U-EVs released from cultures previously exposed to DMSO, ITA, and BARI. The internalization of BARI-, ITA-, and DMSO-J-EVs by circulating leukocytes (neutrophils, monocytes, and lymphocytes) were similar (Fig. 4B and C). Furthermore, there were no significant changes or evidence of a distinct pattern in J-EVs internalization as a function of the jakinib used. Therefore, jakinibs were concluded not to significantly affect J-EV uptake by neutrophils, lymphocytes, or monocytes.

On the other hand, DMSO-U-EVs were ingested by a median of 10 % of neutrophils, 5 % of lymphocytes, and 20 % of monocytes; similar results were observed for BARI-U-EVs (Fig. 4D). Interestingly, higher percentages of leukocytes, *i.e.*, 30 % of neutrophils, 10 % of lymphocytes, and 35 % of monocytes were able to ingest ITA-U-EVs (Fig. 4E). Thus, ITA-U-EVs were internalized approximately twice as much as DMSO-U-EVs (Fig. 4D and E).

Neutrophils and monocytes showed the highest EV ingestion capacity. Moreover, greater internalization (not significant) of EVs by

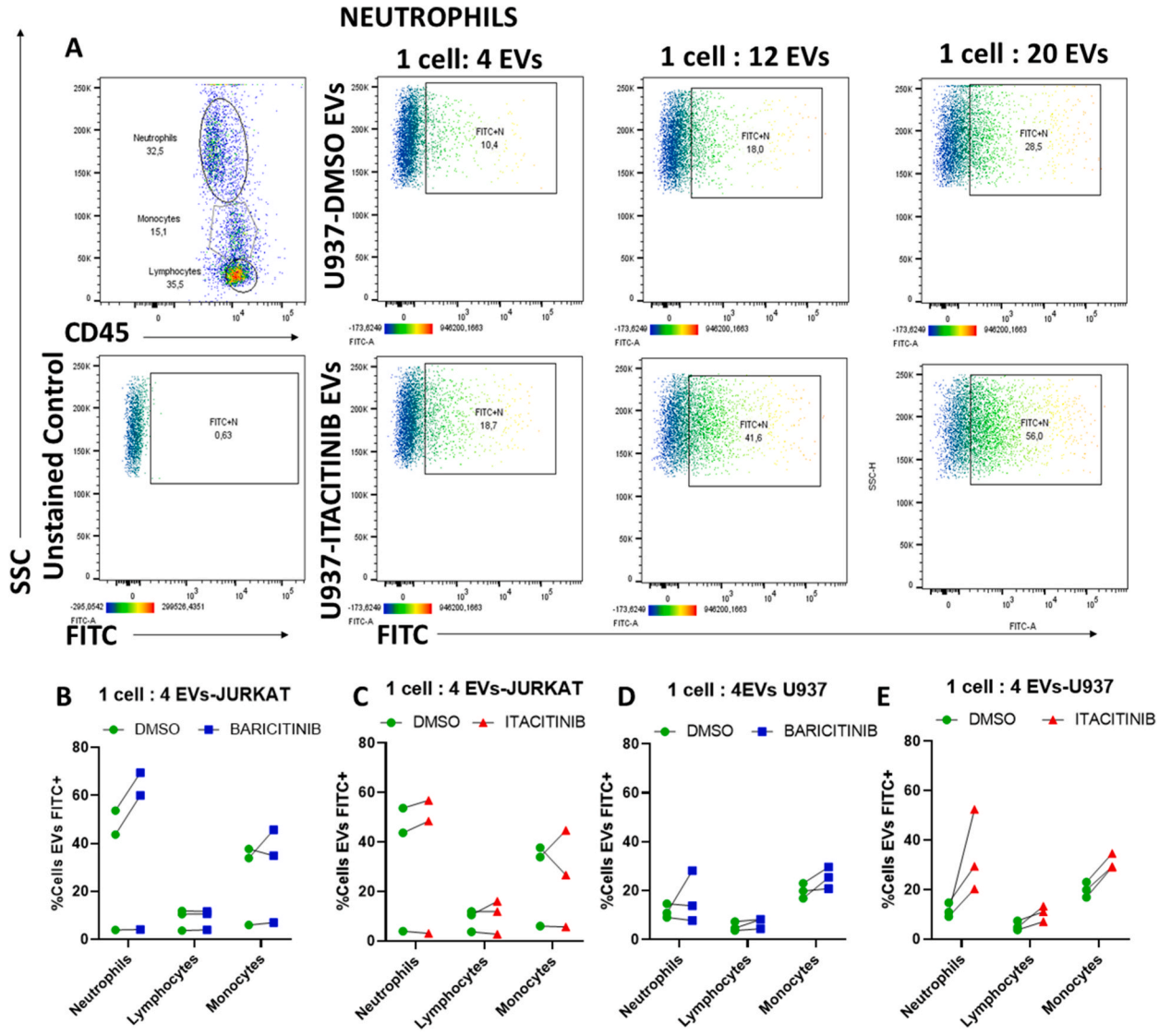

Fig. 4. Peripheral blood leukocytes internalize extracellular vesicles derived from lymphoid and monocytic cell lines. Whole blood samples (187.500 cells approximately) from healthy volunteers were stained with CD45-PeCy7 and incubated with different concentrations of CFSE-labeled EVs released from Jurkat and U937 cells exposed to 0.5 % DMSO, 200 nM bariticinib o 25 μM itacitinib for 24 h. Leukocyte ($CD45^+$ cells) were further discriminated by granularity (SSC–H) to calculate the percentage of CFSE-EV^+-neutrophils, -lymphocytes, and -monocytes after quenching the CFSE fluorescence on the cell surface with trypan blue. **A.** Representative dot plots of DMSO-U-EVs and ITA-U-EVs uptake by neutrophils. Internalization of J-EVs **(B, C)** and U-EVs **(D, E)** by neutrophils, lymphocytes, and monocytes following exposure to baricitinib **(B, D)** or itacitinib **(C, D).** Wilcoxon text for paired groups; n = 3 independent experiments. J: Jurkat, U: U937. (For interpretation of the references to colour in this figure legend, the reader is referred to the Web version of this article.)

each leukocyte subset (monocytes, lymphocytes, and granulocytes) due to the interaction of two critical factors, cell source and treatment, was observed. Given that only the internalization of the ITA-U-EVs was superior to that of DMSO-U-EVs, BARI-U-EVs, and any type of J-EVs, it is possible to conclude that ITA-U-EVs have characteristics that favored their uptake by circulating leukocytes.

3.5. Human monocyte-derived EVs attenuated neutrophil ROS production

Considering the ability of EVs to target various cell types and to elicit various effects, the interaction between EVs and human peripheral blood leukocytes was evaluated.

Since neutrophils internalized J-EVs and U-EVs to a greater extent than lymphocytes and monocytes, the impact of EV uptake on the neutrophil respiratory burst was assessed. Thus, neutrophils previously exposed to L-EVs and M-EVs were stimulated with PMA and incubated with DHR123 to evaluate the respiratory burst by flow cytometry. Notably, neither L-EVs nor M-EVs induced respiratory

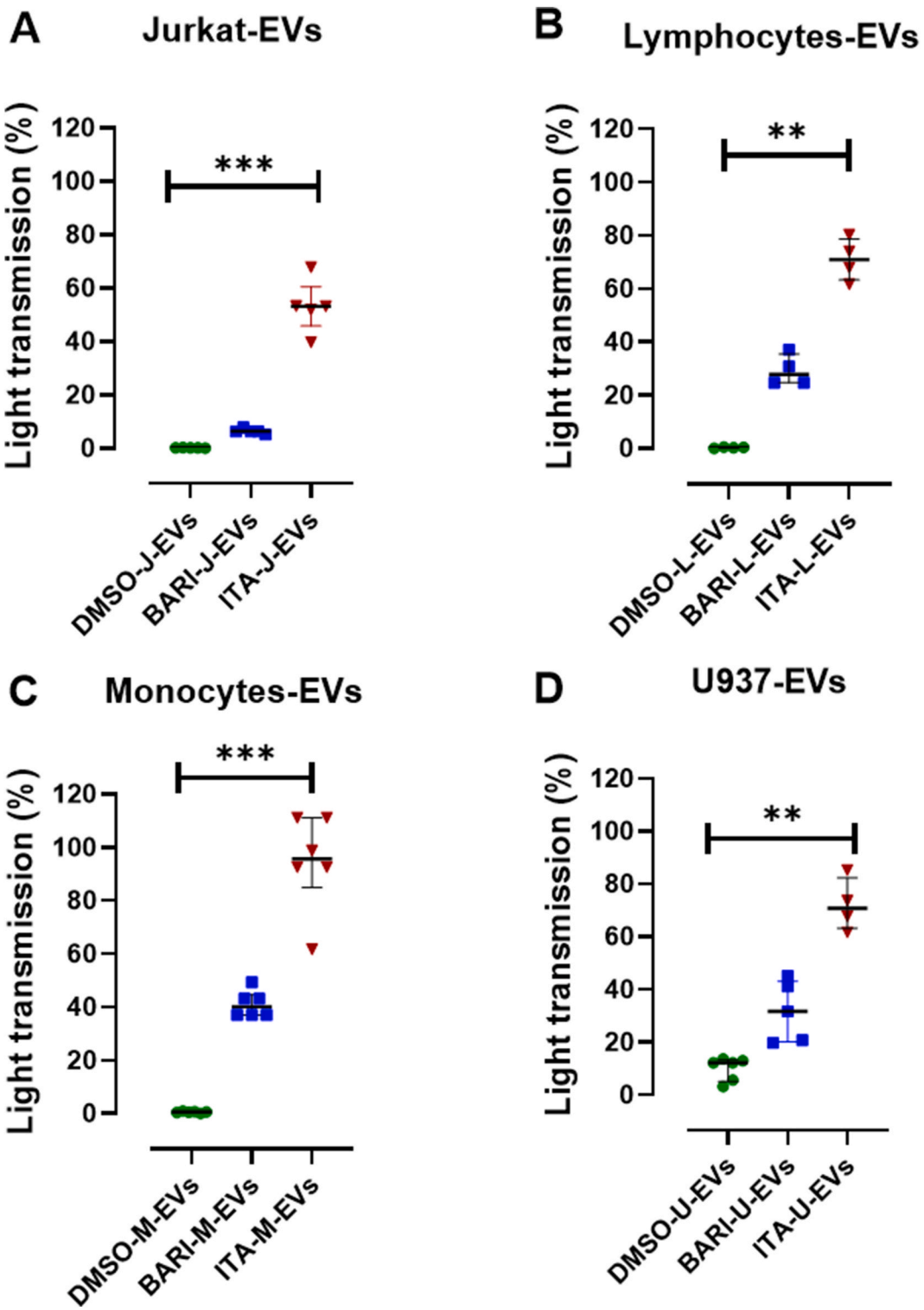

Fig. 5. Effect of extracellular vesicles derived from lymphocytes and monocytes treated with jakinibs on platelet aggregation. Platelet rich plasma samples were exposed to **A.** J-EVs, **B.** L-EVs, **C.** M-EVs and **D.** U-EVs released in the presence of 0.5 % DMSO, 200 nM bariticinib, and 25 μM itacitinib (100 cells: 1250 EVs). After 8 m, percentages of light transmission were measured. Lines represent median ± IQR. *$p < 0.05$; **$p < 0.01$; ***$p < 0.001$; Kruskal Wallis and post-hoc Dunn's tests; $n = 5$ independent experiments. J: Jurkat, L: Lymphocytes, M: Monocytes, U: U937.

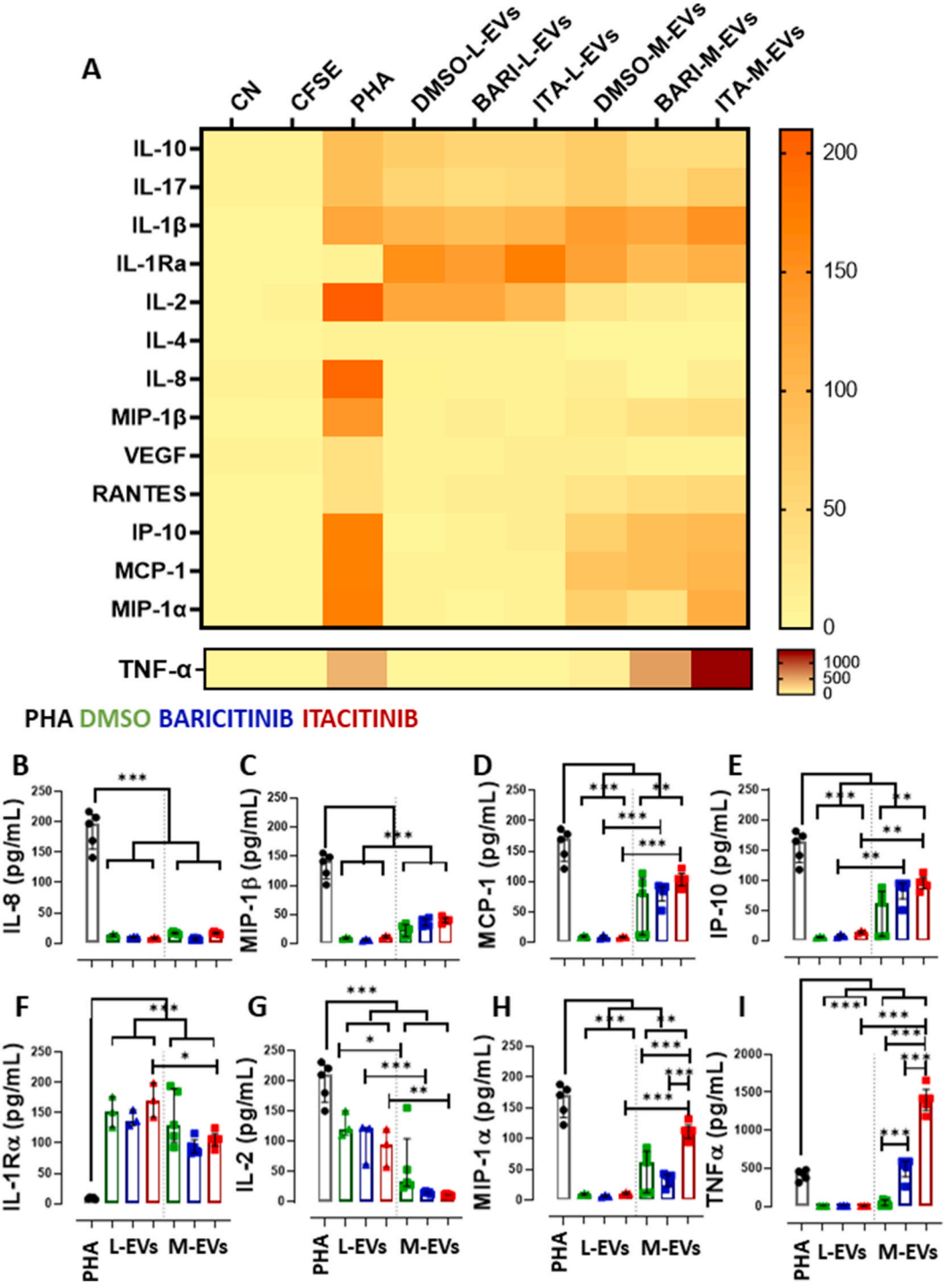

Fig. 6. Effect of extracellular vesicles derived from lymphocytes and monocytes treated with jakinibs on cytokine accumulation in PHA-stimulated PBMC cultures. 1×10^5 CFS-labeled PBMCs from healthy donors were stimulated with 4 % v/v PHA (0.1 mg/ml) in the presence of autologous L-EVs (n = 3) and M-EVs (n = 5) released under treatment with 0.5 % DMSO, 25 μM itacitinib, and 200 nM bariticinib (100 cells: 1250 EVs). Culture supernatants were collected at 6 h and levels of cytokine were quantified by Luminex®Multiplex Assay. **A.** Heat map representing the accumulation of cytokines in every experimental condition. **B.** Bar charts represent concentration (median ± IQR) of IL-8, **C.** MIP-1β, **D.** MCP-1, **E.** IP-10, **F.** IL-1Ra, **G.** IL-2, **H.** MIP-1α, and **I.** TNF-α. *$p < 0.05$; **$p < 0.01$; ***$p < 0.001$; two-way ANOVA and Bonferroni post-hoc tests. CN: negative control, CFSE: CFSE control without stimulus.

burst in neutrophils (Supplementary Figs. S5A, S5B, and S5D). Furthermore, PMA-induced ROS production remained relatively unaltered in neutrophils previously exposed to DMSO-L-EVs (119 %) or ITA-L-EVs (109 %). However, a non-significant decrease was observed in the presence of BARI-L-EVs (87 %) (Fig. S5C). Similarly, PMA-induced ROS production showed a non-significant decrease in the presence of DMSO-*M*-EVs (60 %), BARI-*M*-EVs (83 %), and ITA-*M*-EVs (41 %) (Supplementary Fig. S5E). Collectively, these data indicated that M-EVs can attenuate the neutrophil respiratory burst more than L-EVs (Supplementary Figs. S5C and S5E), suggesting that the cellular source of EVs may modulate ROS generation. In addition, ITA-*M*-EVs were more effective in suppressing the neutrophil respiratory burst than DMSO-*M*-EVs and BARI-*M*-EVs. Similarly, in two out of three experiments, BARI-L-EVs reduced neutrophil respiratory burst more than DMSO-L-EVs and ITA-L-EVs. In summary, the cellular origin and culture conditions under which EVs are released confer specific characteristics that contribute to attenuating the neutrophil respiratory burst.

3.6. M-EVs released in the presence of jakinibs tend to modulate T-cell proliferation

Considering the ability of lymphocytes to bind and internalize EVs, the impact of these vesicles on lymphocyte functionality, particularly on PHA-stimulated T-cells, was evaluated. CFSE-labeled PBMCs were stimulated with PHA and exposed to autologous EVs released from highly purified lymphocytes and monocytes cultured in the presence of the jakinibs.

T-cell proliferation in PHA-stimulated cultures exposed to DMSO-L-EVs and DMSO-*M*-EVs was set as 100 %. Notably, L-EVs had no discernible effect on $CD4^+$ or $CD8^+$ T-cell proliferation (Supplementary Fig. S6A). In contrast, ITA-*M*-EVs induced a non-significant decrease in $CD3^+$ (up to 75 %), $CD4^+$ (up to 85 %), and $CD8^+$ (up to 90 %) T-cell proliferation (Supplementary Fig. S6B). Interestingly, increased T-cell proliferation (110 % for $CD4^+$ T-cells and 130 % for $CD8^+$ T-cells) was observed in the presence of BARI-*M*-EVs. These findings indicated a likely differential immunomodulatory effect of EVs on T-cell functionality, influenced by the cellular source of EVs and the presence of jakinibs during vesicle generation.

To rule out the possibility that the effects attributed to vesicles were due to residual concentrations of jakinibs in the vesicle suspensions, EVs were thoroughly washed with filtered RPMI to reduce the concentration of inhibitors by tenfold compared to vesicle preparations (25 μM ITA and 200 nM BARI). Additional proliferation assays were then carried out with PHA-stimulated PBMCs exposed to these lower inhibitor concentrations. Linear regression analyses were done to assess dose-dependent effects. The slopes of the regression lines were not statistically different from zero for both ITA ($p = 0.3316$) and BARI ($p = 0.1856$) (Supplementary Fig. S7 A and B). These findings confirmed that the modulation of T-cell proliferation observed in the presence of EVs, could undoubtedly be attributed to EVs and not to residual jakinibs present in vesicle suspensions.

In addition, we evaluated the expression of CD69 and CD25 on T-cells in PHA-stimulated PBMC cultures exposed to different types of EVs for 96 h. The MFI values of CD69 and CD25 of cultures exposed to DMSO-L-EVs and DMSO-*M*-EVs were set as 100 % marker expression. These vesicles did not significantly alter CD69 or CD25 expression on T-cells compared to PHA-stimulated control cultures (Supplementary Figs. S6A and S6B). However, a non-significant decrease in CD25 expression was observed in the presence of ITA-L-EVs (68 %) and ITA-*M*-EVs (56 %) (Supplementary Figs. S6A and S6B), possibly related to the lower T-cell proliferation observed in cultures exposed to these EVs. In contrast, BARI-*M*-EVs induced higher expression of CD25 (29 %) compared to DMSO-*M*-EVs (Supplementary Fig. S6B), consistent with the increased proliferation of $CD3^+$, $CD4^+$, and $CD8^+$ T-cells in the presence of these type of vesicles.

3.7. Extracellular vesicles derived from lymphocytes and monocytes treated with itacitinib promote platelet aggregation

PRP samples were exposed to L-EVs, J-EVs, M-EVs, and U-EVs generated in the presence of DMSO, BARI, and ITA to evaluate their impact on platelet aggregation by LTA. Compared with control DMSO-EVs, platelet aggregation increased significantly in the presence of ITA-J-EVs ($p < 0.001$, Fig. 5A), ITA-L-EVs ($p < 0.01$, Fig. 5B), ITA-*M*-EVs ($p < 0.001$, Fig. 5C), and ITA-U-EVs ($p < 0.001$, Fig. 5D).

A slight increase in platelet aggregation was also observed in PRP samples exposed to BARI-L-EVs (30 %) and BARI-*M*-EVs (40 %) (Fig. 5B and C) compared with DMSO-EVs. Importantly, neither BARI nor ITA directly affected platelet aggregation, as their percent light transmission values resembled those of DMSO controls (data not shown).

Furthermore, EVs derived from monocytic cells exposed to jakinibs, ITA-U-EVs and ITA-*M*-EVs, displayed a greater capacity to activate platelet aggregation, reaching 70 % and 90 % values, respectively, compared with 50 % and 70 % when exposed to lymphoid cells, ITA-J-EVs and ITA-L-EVs, respectively. Although the type of jakinib was the primary factor influencing platelet aggregation, the cell source of EVs also played a role, albeit no significant interaction between the two factors was observed.

3.8. Extracellular vesicles derived from lymphocytes and monocytes treated with jakinibs modulate cytokine accumulation in PHA-stimulated PBMC cultures

The effect of EVs generated in the presence of jakinibs on the immune response was evaluated by quantifying cytokines accumulated in PHA-stimulated PBMC cultures. For this purpose, CFSE-labeled PBMC were stimulated with PHA (0.1 mg/ml) and exposed to autologous EVs generated in the presence of DMSO, BARI, and ITA. The levels of pro- and anti-inflammatory cytokines in supernatants collected 6 h after PHA treatment and exposure to the different autologous EVs were determined by Luminex assays. Interleukin-10, IL-1β, IL-17, IL-4, RANTES, and VEGF levels remained similar in cultures incubated with EVs, regardless of their cellular origin or the specific jakinib used (Fig. 6A). Thus, neither the cellular origin of EVs nor the jakinib selected had an apparent impact on the synthesis of these cytokines.

In contrast, the levels of other cytokines (IL-8, MIP-1β, MCP-1, IP-10, IL-2, MIP-1α, and TNFα) increased in PHA-stimulated PBMC

cultures not exposed to EVs. However, the presence of any type of EVs resulted in a decreased level of these cytokines. In particular, IL-8 levels diminished in the presence of L-EVs ($p < 0.001$) and M-EVs ($p < 0.001$), regardless of the cellular source or the jakinib used (Fig. 6A and B). MIP-1β was significantly decreased by 95 % in the presence of L-EVs ($p < 0.01$) and by 70 % with M-EVs ($p < 0.001$) (Fig. 6C). Similar trends were observed for MCP-1 and IP-10 in cultures exposed to L-EVs ($p < 0.001$) and M-EVs ($p < 0.01$) (Fig. 6E). Furthermore, IL-2 was significantly reduced in the presence of L-EVs ($p < 0.001$) and more prominently in the case of M-EVs ($p < 0.001$) (Fig. 6F), suggesting that the cellular source of EVs had a more pronounced modulatory effect on MCP-1 (Fig. 6D), IP10 (Fig. 6E), and IL-2 levels than the jakinib used during EV generation.

On the other hand, IL-1Ra levels did not increase in PHA-stimulated PBMC cultures but increased in response to L-EVs ($p < 0.001$) and M-EVs ($p < 0.001$) (Fig. 6G). Indeed, DMSO-L-EVs, BARI-L-EVs, and ITA-L-EVs induced IL-1Ra accumulation to a greater extent than their monocytic counterparts ($p < 0.05$; Fig. 6G). In contrast, MIP-1α and TNF-α levels were modulated by EVs in a manner dependent on their cellular origin and the specific jakinib present during their generation. Lymphocyte-derived EVs displayed a more pronounced effect on MIP-1α and TNFα levels than M-EVs. MIP-1α concentrations decreased in the presence of L-EVs ($p < 0.001$) and M-EVs ($p < 0.01$) (Fig. 6H). Similarly, TNF-α levels decreased in cultures exposed to L-EVs ($p < 0.001$) and, to a lesser extent, to M-EVs, except in the case of DMSO-*M*-EVs, which significantly reduced the levels of this cytokine (Fig. 6I).

Additionally, MIP-1α levels were significantly reduced in the presence of DMSO-*M*-EVs ($p < 0.001$) and BARI-*M*-EVs ($p < 0.01$), in comparison with ITA-*M*-EVs (Fig. 6H). In contrast, TNF-α levels were 10-fold higher in the presence of ITA-*M*-EVs when compared with DMSO-*M*-EVs ($p < 0.001$), BARI-*M*-EVs ($p < 0.001$), and ITA-L-EVs ($p < 0.001$) (Fig. 6I). These findings highlighted that the cellular

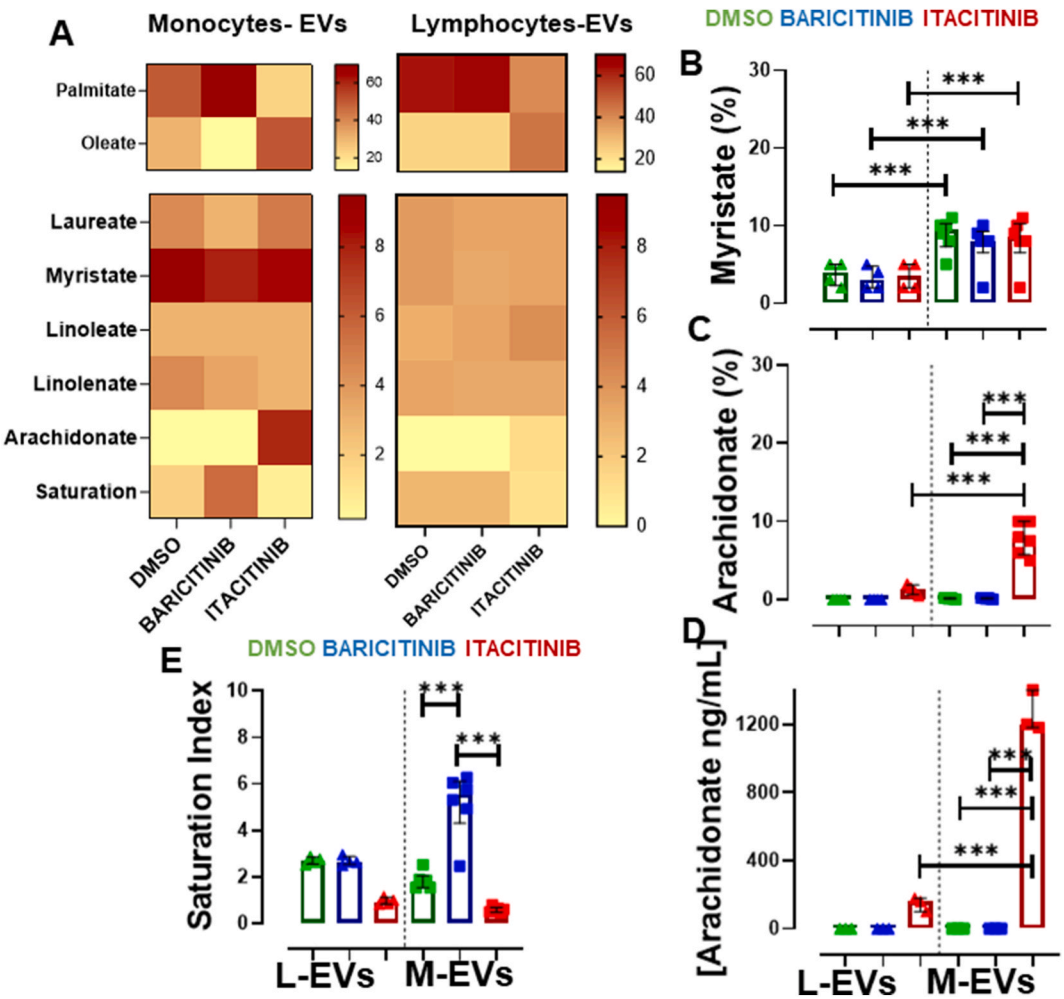

Fig. 7. Fatty acid profile of extracellular vesicles derived from lymphocytes and monocytes treated with jakinibs. Extracellular vesicles were isolated from sorted monocytes and lymphocytes cultured in the presence of 0.5 % DMSO, 200 nM bariticinib, 25 μM itacitinib. **A.** The heat map represents the fatty acid composition and the fatty acid saturation index of the EVs. Bar charts represent the median ± IQR percentages of myristate **(B)**, arachidonate **(C)**, arachidonate detected by ELISA **(D)** and the fatty acid saturation index of the EVs **(E)**. *$p < 0.05$; **$p < 0.01$; ***$p < 0.001$; Kruskal-Wallis and post-hoc Dunn's tests. L-EVs: n = 3 independent experiments. M-EVs: n = 5 independent experiments. L-EVs: lymhocyte-derived EVs M-EVs: monocyte-derived EVs.

origin of EVs and the specific jakinib present during their generation had a significant role in the modulatory effect of EVs on MIP-1α and TNF-α levels.

3.9. Jakinibs modulate the fatty acid content of extracellular vesicles

Fatty acids are structural components of cell membranes and have functional roles in cell signaling. The FA composition of EVs can influence their biological functions. Specific FA are involved in the regulation of inflammation, immune responses, and other biological processes. Studying the FA profile of EVs, provides researchers with insights into the potential functional roles of these vesicles in various physiological and pathological contexts.

The FA profile of EVs, generated under different experimental conditions, was analyzed by FAME derivatization followed by GC. The heat map (Fig. 7A) shows the variation of the FA content of EVs as a function of cell lineage and jakinib present during their generation. M-EVs were found to contain a significantly higher proportion of myristate compared with L-EVs ($p < 0.011$), as depicted in Fig. 7B. Furthermore, ITA-*M*-EVs exhibited a significantly higher arachidonate content than DMSO-*M*-EVs ($p < 0.001$) and BARI-*M*-EVs ($p < 0.001$), as shown in Fig. 7C. Although not statistically significant, a trend towards increased arachidonate content was observed in ITA-L-EVs than in DMSO-L-EVs (Fig. 7C).

Additionally, a commercial ELISA kit was used to determine the concentration of AA in EV-derived lysates, to analyze the EVs' AA content from a different perspective. The AA concentrations of vesicle lysates showed a similar profile to that evidenced through GC-FAME, as shown in Fig. 7D.

Analyses of the fatty acid saturation index (FA-SI) showed a higher proportion of saturated FAs in BARI-*M*-EVs than in DMSO-*M*-EVs ($p < 0.001$) and ITA-*M*-EVs ($p < 0.001$) (Fig. 7E). Interestingly the SI values for ITA-*M*-EVs and ITA-L-EVs were slightly lower than in their respective DMSO controls. No significant differences were found in the proportions of oleate, palmitate, linoleate, linolenate, and laurate in the different EVs (Fig. 7A).

Additionally, the FA profile was analyzed in EVs isolated by two different methods to evaluate the possible effect of such strategies on the features of EVs. For this purpose, U-EVs released in cultures under different treatments were isolated by the standard high-speed centrifugation method and a size exclusion chromatography approach. Particles were similar in size as evidenced by the DLS patterns (Figs. S8A and S8B), and the FA profiles were analyzed by GC using a FAME column. Although the FA profiles were overall similar, a highest variability in arachidonate, palmitate, and oleate amounts was observed when FAs were extracted from EVs using the FAME column (Figs. S8C and S8D).

4. Discussion

Janus kinase inhibitors are beneficial in treating autoimmune diseases, GVHD [59], and cancer. ITA and BARI, though generally well-tolerated, can cause side effects such as thrombosis, lymphocytosis, and neutropenia [20,60–62]. Emerging evidence suggests that EVs are crucial in platelet aggregation and coagulation disorders. They can interact directly with platelets, inducing activation and aggregation. For instance, EVs released by activated endothelial cells or leukocytes can bind to platelet receptors (P-selectin and GPIIb/IIIa), promoting adhesion and aggregation. In addition, EVs can enhance platelet activation by releasing bioactive molecules such as tissue factor and arachidonic acid [63]. The present study focused on the immunomodulatory effects of EVs derived from myeloid and lymphoid cells exposed to ITA and BARI.

The cellular uptake of EVs varies according to cell type. EVs generated in the presence of jakinibs, especially lymphoid and monocytic origin, are more easily internalized by neutrophils and monocytes due to the specific receptors expressed by these phagocytic cells [64,65]. The high phagocytic activity of neutrophils and monocytes, and their role in clearing material released by dying cells, contributes to their ability to take up EVs efficiently [66]. In contrast, lymphocytes have a lower EV uptake capacity, which is furthermore different between B-cells and T-cells given their differential endocytic activity. Monocytes are the leukocytes with the highest EV uptake capacity [67]. Previous research from our group has also found that monocytes ingest EVs more efficiently than lymphocytes [68]. Furthermore, evidence support that EV uptake by peripheral blood leukocytes is also affected by the cellular origin of the vesicles [65,69].

We observed that neutrophils, monocytes, and lymphocytes tend to ingest more ITA-U-EVs than DMSO-U-EVs. This observation suggests that the FA composition of the vesicle membranes may influence the mechanisms of their cellular uptake. Some vesicles with long-chain polyunsaturated FA may promote their endocytosis through specific receptor-mediated pathways, whereas others may be internalized through less regulated processes. The higher proportion of unsaturated FA in M-EVs released under ITA treatment could be related to changes in membrane fluidity [70,71].

The proportion of unsaturated FAs in EVs might be related to their effect on the respiratory burst of neutrophils. Indeed, ROS production decreased when neutrophils were exposed to ITA-*M*-EVs and DMSO-*M*-EVs. Moreover, this effect correlated with a lower FA-SI and a higher content of unsaturated FA, such as arachidonate (C20:4) and oleate (C18:1) within the vesicles. Furthermore, pretreatment of neutrophils with BARI-L-EVs and ITA-L-EVs resulted in reduced ROS production, consistent with increased oleate, linoleate (C18:2), and linolenate (C18:3) content within the vesicles. These findings support previous research on the antioxidant properties of polyunsaturated FAs [72–76]. For instance, Richard et al. demonstrated that different FAs could modulate ROS production by human aortic epithelial cells. Arachidonate micelles (5 μM) reduced ROS production by 45.6 ± 2 %, whereas oleate and linoleate inhibited superoxide anion production by 25.5 ± 3.4 % and 37.4 ± 2.8 %, respectively. Significantly, higher levels of unsaturated FAs were associated with lower ROS production [72]. Even at a lower concentration (3.3 μM), AA protected embryoid body formed from pluripotent stem cells from ROS damage and cell death [75].

Similarly, in murine macrophage cultures, the PMA-induced respiratory burst decreased when the media was supplemented with linoleate and linolenate (at a ratio of 10:1 or 1:10) in a dose-dependent manner [73]. These results may be attributed to the mechanism described by Massaro et al., suggesting that FA unsaturation was related to inhibition of cytochrome C reduction and, consequently, ROS synthesis reduction [74]. Saffaryazdi et al. found that there was a high and positive correlation (Pearson's correlation coefficient analysis) between the amounts of α-linolenic acid and linoleic acid and antioxidant activity assessed by DPPH (2,2-diphenyl-1-picrylhydrazyl) [76]. However, other studies have shown that oleate, linoleate, linolenate, and arachidonate can induce ROS production dose-dependently [77,78].

It's important to note that the results concerning the respiratory burst were obtained from experiments with sodium salts of FAs and not with EVs containing FAs. Therefore, other factors and interactions may be involved, and some complex aspects remain unknown. For instance, in addition to unsaturated FAs, EVs may contain antioxidant agents like SOD2 and catalase [79]. Exosomes derived from peroxide-exposed granulocytes have been found to contain elevated levels of Nrf2 and antioxidants such as catalases, peroxiredoxins, and thioredoxins [80,81]. All these proteins help mitigate the effects of the respiratory burst.

We also studied the effect of EVs on PHA-induced T-cell responses. We found no statistically significant reduction in $CD3^+$, $CD4^+$, or $CD8^+$ T-cell proliferation in cultures exposed to EVs. Moreover, CD69 expression on T cells remained constant in all treatment groups. These findings indicated that the EVs had no inhibitory effects on PHA-induced T-cell activation.

In contrast, ITA-L/M-EVs appeared to influence CD25 expression. This effect could be related to the high arachidonate content within the vesicles. Interestingly, previous experiments with T cells co-cultured with dendritic cells pre-treated with an arachidonate ester resulted in reduced T-cell proliferation and lower CD25 expression [82]. These findings are consistent with the reduced IL-2 levels detected in cultures exposed to ITA-*M*-EVs.

Fatty acids can also influence T-cell proliferation in a dose-dependent manner [83]. Specifically, palmitate, oleate, stearic acid, and linoleate have been shown to reduce T-cell proliferation by decreasing IL-2 synthesis [84]. In the present study, we found higher concentrations of oleate and linoleate in ITA-L/M-EVs, which showed more potent inhibitory effects on T-cell proliferation. To inhibit T-cell proliferation, the concentration of oleate and linoleate apparently should be close to 50 μM. Consequently, it can be deduced that EVs do not affect T-cell activation but negatively regulate T-cell proliferation by reducing IL-2 levels and CD25 expression. Of note, in addition to FAs, some EVs may contain molecules such as arginase I or FasL that can inhibit T-cell proliferation [37,85]. FasL promotes T-cell death, whereas arginase I reduces the expression of the CD3 zeta-chain on T cells, thereby inhibiting their activation [85].

Treatment of PHA-stimulated PBMCs with DMSO-L/M-EVs and Jakinib-L/M-EVs significantly reduced significantly the level of several pro-inflammatory cytokines, including IL-8, MIP-1β, IL-2, IP-10, MCP-1, and MIP-1α, as shown in Fig. 6. In general, the reduction vas more significant in cultures exposed to L-EVs than M-EVs, except for IL-2, which decreased to a greater extent in the presence of M-EVs. On the other hand, all types of EVs consistently induced an increased accumulation of the anti-inflammatory cytokine IL-1Rα.

Interestingly, L-EVs were found to reduce the TNF-α levels while simultaneously promoting the accumulation of IL-1Ra. In contrast, M-EVs tended to favor an increase in TNF-α and raised IL-1Ra levels, although to a lesser extent than L-EVs. These observations suggested that L-EVs have more anti-inflammatory activity than M-EVs. This difference could be attributed to the higher myristate content in M-EVs. Notably, the gene expression of TNF-α, MCP-1, and IL-6 was increased in murine 3T3-L1 preadipocytes exposed 6 h to 0.5 μM myristate complexed with albumin [86]. Although no previous evidence supports the elevation of MIP-1β, IP-10, and MIP-1α levels following myristate exposure, it is plausible to suggest that this FA could be responsible for the increased accumulation of these other pro-inflammatory chemokines. Therefore, further studies on myristic acid are warranted.

Furthermore, it's worth mentioning that within the M-EV group, BARI/ITA-*M*-EVs induced a more substantial accumulation of MIP-1β, MCP-1, IP-10, MIP-1α, and TNF-α. This observation underscores that the inhibitory effects of these vesicles on the accumulation of pro-inflammatory cytokines are not solely dependent on their cellular origin but are also influenced by jakinib exposure. ITA and BARI appear to alter the features of the vesicles, enabling them to modulate cytokine levels in culture. It is essential to remember that EVs can exert enhancing and inhibitory effects on cytokine accumulation. These opposing effects could be associated with their lipid composition and their cargos [87].

Although we have identified variable levels of some cytokines in the supernatants analyzed, probably related to EV-dependent modulation, this research can only scratch the surface of their true significance. Cytokines play a critical role in cellular communication and regulation of immune responses. Normally, when released, cytokines bind to specific receptors on target cells, initiating a wide range of cellular reactions [88]. However, it's essential to consider that, in some cases, cytokines can bind to soluble receptors, which can deeply affect immune and inflammatory responses. These effects may include the neutralization of cytokine activity and attenuation of the responses they mediate due to the sequestration of cytokines with soluble receptors. This regulatory effect serves as a natural feedback mechanism to prevent uncontrolled responses and probably alters the half-life of cytokines [88].

When evaluating the effect of EVs on platelets, it was found that ITA-L/M-EVs increased platelet aggregation. This result may be associated with vesicles' higher arachidonate and lower linoleate proportions. Since platelets can endocytose EVs [89,90], the vesicular arachidonate could induce platelet aggregation [40,91]. In fact, at low concentrations (2 μg/mL), arachidonate can induce platelet activation and phosphatidylserine exposure and promote a procoagulant state [92]. In addition, cyclooxygenase-1 can convert arachidonate into thromboxane A2 (TxA2) [93,94], thus amplifying the vesicular arachidonate effects [95–97].

Finally, given the increasing availability of EV isolation methods, we evaluated the variations of some critical parameters of EVs isolated by centrifugation and size exclusion chromatography. In particular, the FA profile and the ability to promote platelet aggregation were evaluated. Interestingly, no significant differences attributable to the isolation methods were observed (Supplementary Fig. S8). However, it is noteworthy that size exclusion chromatography showed a higher efficiency in the recovery of EVs than the centrifugation-based method.

In conclusion, this study has provided valuable information on L/M-EVs generated in the presence of Janus kinase inhibitors. The lipid composition of these EVs varied depending on their cellular origin and the jakinib used during their generation. They were predominantly ingested by neutrophils and showed different effects on peripheral blood cells. ITA-L/M-EVs reduced ROS production by PMA-activated neutrophils by a mechanism likely attributable to their higher proportion of unsaturated FAs. Furthermore, ITA-L/M-EVs increased platelet aggregation, an effect that could be related to their high arachidonate content. Additionally, ITA-*M*-EVs were found to contain substantial proportions of oleate and linoleate, both known inhibitors of T-cell proliferation. Surprisingly, L/M-EVs, particularly L-EVs, attenuated the levels of pro-inflammatory chemokines and cytokines in PHA-stimulated PBMC cultures. This effect is possibly associated with a lower myristate fraction in L-EVs, highlighting the pivotal role of the cellular source of EVs in their downstream effects. All these findings underline the complexity of the composition of EVs and their potential impact on immune responses and intercellular communication.

4.1. Perspectives

This study revealed the complex role of Jakinib-L/M-EVs in intercellular communication and immune responses, suggesting avenues for future research:

Investigating neutrophil-EV interaction: Understanding how neutrophils preferentially uptake Jakinib-L/M-EVs may lead to targeted therapeutic strategies.

Analyzing the impact of EV lipid composition on immune response: Identifying specific lipids responsible for immune modulation may help design lipid-based immunomodulatory therapies.

Exploring EV-mediated ROS and platelet regulation: Investigating the connections between EV lipid content, neutrophil ROS production, and platelet aggregation may have therapeutic implications for inflammatory and thrombotic conditions.

Studying the effects of oleate and linoleate on T-cell proliferation: Investigating how these ITA-*M*-EVs lipids influence T-cell function could lead to novel immunomodulatory approaches.

Understanding EV-mediated immune suppression: Investigating the signaling pathways involved in the suppression of pro-inflammatory molecules by L/M-EVs could lead to therapies for dampen excessive inflammation.

Data availability statement

The data that support the findings of this study are available upon reasonable request from the corresponding author. Researchers interested in accessing the data can contact Mauricio Rojas via email at mauricio.rojas@udea.edu.co.

Funding

Ministry of Science, Technology and Innovation of Colombia (Minciencias Code 111584467267 - Contract 925-2019 and UdeA Sostenibilidad-CODI) .

CRediT authorship contribution statement

Ana María Daza Zapata: Writing – review & editing, Writing – original draft, Methodology, Formal analysis, Data curation, Conceptualization. **Karen Álvarez:** Writing – review & editing, Writing – original draft, Methodology, Investigation, Formal analysis, Conceptualization. **Gloria Vásquez Duque:** Writing – original draft, Supervision, Investigation, Conceptualization. **Juliana Palacio:** Writing – original draft, Methodology, Investigation. **Mauricio Rojas López:** Writing – review & editing, Writing – original draft, Visualization, Supervision, Resources, Project administration, Methodology, Investigation, Funding acquisition, Formal analysis, Data curation, Conceptualization.

Declaration of competing interest

The authors declare the following financial interests/personal relationships which may be considered as potential competing interests:Mauricio Rojas Lopez reports financial support (Minciencias Code 111584467267 - Contract 925-2019 and UdeA Sostenibilidad-CODI), statistical analysis, travel, and publication support were provided by University of Antioquia. Mauricio Rojas Lopez reports a relationship with University of Antioquia that includes: employment. In relation to potential conflicts of interest, I want to declare that I currently hold no editorial positions in any journal, and my primary professional activity is teaching in the field of Immunology at the Faculty of Medicine. I have no financial relationships or direct collaborations with the authors involved in this manuscript, and my involvement in the review will be solely based on the scientific quality of the presented work.I am committed to ensuring an impartial and objective evaluation of this manuscript, without undue influence from any relationship or activity that could be perceived as a conflict of interest. If there are other authors, they declare that they have no known competing financial interests or personal relationships that could have appeared to influence the work reported in this paper.

Acknowledgements

We thank Marta Mesa for her English Language Wording review and correction.

Appendix A. Supplementary data

Supplementary data to this article can be found online at https://doi.org/10.1016/j.heliyon.2024.e24710.

References

[1] J.J. O'Shea, et al., The JAK-STAT pathway: impact on human disease and therapeutic intervention, Annu. Rev. Med. 66 (2015) 311–328, https://doi.org/10.1146/annurev-med-051113-024537. D.O.I:.

[2] S.J. Thomas, J.A. Snowden, M.P. Zeidler, S.J. Danson, The role of JAK/STAT signalling in the pathogenesis, prognosis and treatment of solid tumours, Br. J. Cancer 113 (2015) 365–371, https://doi.org/10.1038/bjc.2015.233. D.O.I:.

[3] L.J. Qiu, et al., Decreased SOCS1 mRNA expression levels in peripheral blood mononuclear cells from patients with systemic lupus erythematosus in a Chinese population, Clin. Exp. Med. 15 (2015) 261–267, https://doi.org/10.1007/s10238-014-0309-2. D.O.I:.

[4] H.E. Sabaawy, B.M. Ryan, H. Khiabanian, S.R. Pine, JAK/STAT of all trades: linking inflammation with cancer development, tumor progression and therapy resistance, Carcinogenesis 42 (2021) 1411–1419, https://doi.org/10.1093/carcin/bgab075. D.O.I:.

[5] A.J. Brooks, T. Putoczki, JAK-STAT signalling pathway in cancer, Cancers 12 (2020), https://doi.org/10.3390/cancers12071971.

[6] A. Lescoat, et al., Combined anti-fibrotic and anti-inflammatory properties of JAK-inhibitors on macrophages in vitro and in vivo: Perspectives for scleroderma-associated interstitial lung disease, Biochem. Pharmacol. 178 (2020) 114103, https://doi.org/10.1016/j.bcp.2020.114103. D.O.I:.

[7] S. Kubo, S. Nakayamada, Y. Tanaka, Baricitinib for the treatment of rheumatoid arthritis and systemic lupus erythematosus: a 2019 update, Expet Rev. Clin. Immunol. 15 (2019) 693–700, https://doi.org/10.1080/1744666X.2019.1608821. D.O.I:.

[8] K. Meesilpavikkai, et al., Efficacy of baricitinib in the treatment of Chilblains associated with Aicardi-Goutieres syndrome, a type I interferonopathy, Arthritis Rheumatol. 71 (2019) 829–831, https://doi.org/10.1002/art.40805. D.O.I:.

[9] C.C. Mok, The Jakinibs in systemic lupus erythematosus: progress and prospects, Expert Opin Investig Drugs 28 (2019) 85–92, https://doi.org/10.1080/13543784.2019.1551358. D.O.I:.

[10] C.O. Bingham (Ed.), Conversion of FACIT-F to PROMIS(R) Fatigue Scores in Two Phase 3 Baricitinib Rheumatoid Arthritis Trials, 3rd, Arthritis Care Res (Hoboken)., 2020, https://doi.org/10.1002/acr.24144.

[11] K. Michaud, et al., Relative impact of pain and fatigue on work productivity in patients with rheumatoid arthritis from the RA-BEAM baricitinib trial, Rheumatol Ther 6 (2019) 409–419, https://doi.org/10.1007/s40744-019-0164-4. D.O.I:.

[12] Y. Li, et al., Changes in serum cytokines may predict therapeutic efficacy of tofacitinib in rheumatoid arthritis, Mediators Inflamm (2019) 5617431, https://doi.org/10.1155/2019/5617431, 2019.

[13] T. Dorner, et al., Baricitinib decreases anti-dsDNA in patients with systemic lupus erythematosus: results from a phase II double-blind, randomized, placebo-controlled trial, Arthritis Res. Ther. 24 (2022) 112, https://doi.org/10.1186/s13075-022-02794-x. D.O.I:.

[14] M. Yamamoto, et al., Tofacitinib can decrease anti-DNA antibody titers in inactive systemic lupus erythematosus complicated by rheumatoid arthritis, Mod. Rheumatol. 26 (2016) 633–634, https://doi.org/10.3109/14397595.2015.1069473. D.O.I:.

[15] J. Kremer, T.W.J. Huizinga, L. Chen, C.G. Saifan, M. Issa, S.L. Witt, I. de la Torre, FRI0090 Analysis of neutrophils, lymphocytes, and platelets in pooled phase 2 and phase 3 studies of Baricitinib for rheumatoid arthritis, Ann. Rheum. Dis. 76 (2017) 512, https://doi.org/10.1136/annrheumdis-2017-eular.1325. D.O.I:.

[16] Y. Tanaka, et al., Characterization and changes of lymphocyte subsets in baricitinib-treated patients with rheumatoid arthritis: an integrated analysis, Arthritis Rheumatol. 70 (2018) 1923–1932, https://doi.org/10.1002/art.40680. D.O.I:.

[17] J. Kay, et al., Changes in selected haematological parameters associated with JAK1/JAK2 inhibition observed in patients with rheumatoid arthritis treated with baricitinib, RMD Open 6 (2020), https://doi.org/10.1136/rmdopen-2020-001370. D.O.I:.

[18] Y. Tanaka, et al., Efficacy and safety of baricitinib in Japanese patients with active rheumatoid arthritis: a 52-week, randomized, single-blind, extension study, Mod. Rheumatol. 28 (2018) 20–29, https://doi.org/10.1080/14397595.2017.1307899. D.O.I:.

[19] D.J. Wallace, et al., Baricitinib for systemic lupus erythematosus: a double-blind, randomised, placebo-controlled, phase 2 trial, Lancet 392 (2018) 222–231, https://doi.org/10.1016/s0140-6736(18)31363-1.

[20] K.A. Papp, et al., A randomized phase 2b trial of baricitinib, an oral Janus kinase (JAK) 1/JAK2 inhibitor, in patients with moderate-to-severe psoriasis, Br. J. Dermatol. 174 (2016) 1266–1276, https://doi.org/10.1111/bjd.14403. D.O.I:.

[21] J.G. Kettle, et al., Inhibitors of JAK-family kinases: an update on the patent literature 2013-2015, part 1, Expert Opin. Ther. Pat. 27 (2017) 127–143, https://doi.org/10.1080/13543776.2017.1252753. D.O.I:.

[22] J.O. Mascarenhas, et al., Primary analysis of a phase II open-label trial of INCB039110, a selective JAK1 inhibitor, in patients with myelofibrosis, Haematologica 102 (2017) 327–335, https://doi.org/10.3324/haematol.2016.151126.

[23] G.L. Beatty, et al., A phase ib/II study of the JAK1 inhibitor, itacitinib, plus nab-paclitaxel and gemcitabine in advanced solid tumors, Oncol. 24 (2019) 14-e10, https://doi.org/10.1634/theoncologist.2017-0665.

[24] R. Bissonnette, et al., A randomized, double-blind, placebo-controlled, dose-escalation study of the safety and efficacy of INCB039110, an oral janus kinase 1 inhibitor, in patients with stable, chronic plaque psoriasis, J. Dermatol. Treat. 27 (2016) 332–338, https://doi.org/10.3109/09546634.2015.1115819. D.O.I:.

[25] R. Zeiser, et al., Efficacy and safety of itacitinib versus placebo in combination with corticosteroids for initial treatment of acute graft-versus-host disease (GRAVITAS-301): a randomised, multicentre, double-blind, phase 3 trial, Lancet Haematol 9 (2022) e14–e25, https://doi.org/10.1016/S2352-3026(21)00367-7.

[26] S. Mori, F. Ogata, R. Tsunoda, Risk of venous thromboembolism associated with Janus kinase inhibitors for rheumatoid arthritis: case presentation and literature review, Clin. Rheumatol. 40 (2021) 4457–4471, https://doi.org/10.1007/s10067-021-05911-4. D.O.I:.

[27] P.P. Kulkarni, et al., Fatty acid oxidation fuels agonist-induced platelet activation and thrombus formation: targeting beta-oxidation of fatty acids as an effective anti-platelet strategy, FASEB J 37 (2023) e22768, https://doi.org/10.1096/fj.202201321RR. D.O.I:.

[28] W.J. Lu, et al., Role of a Janus kinase 2-dependent signaling pathway in platelet activation, Thromb. Res. 133 (2014) 1088–1096, https://doi.org/10.1016/j.thromres.2014.03.042. D.O.I:.

[29] S. Koride, S. Nayak, C. Banfield, M.C. Peterson, Evaluating the role of janus kinase pathways in platelet homeostasis using a systems modeling approach, CPT Pharmacometrics Syst. Pharmacol. 8 (2019) 478–488, https://doi.org/10.1002/psp4.12419. D.O.I:.

[30] C. Thery, et al., Minimal information for studies of extracellular vesicles 2018 (MISEV2018): a position statement of the International Society for Extracellular Vesicles and update of the MISEV2014 guidelines, J. Extracell. Vesicles 7 (2018) 1535750, https://doi.org/10.1080/20013078.2018.1535750. D.O.I:.

[31] M. Mathieu, L. Martin-Jaular, G. Lavieu, C. Thery, Specificities of secretion and uptake of exosomes and other extracellular vesicles for cell-to-cell communication, Nat. Cell Biol. 21 (2019) 9–17, https://doi.org/10.1038/s41556-018-0250-9. D.O.I:.

[32] P.D. Stahl, G. Raposo, Extracellular vesicles: exosomes and microvesicles, integrators of homeostasis, Physiology 34 (2019) 169–177, https://doi.org/10.1152/physiol.00045.2018.

[33] L.M. Doyle, M.Z. Wang, Overview of extracellular vesicles, their origin, composition, purpose, and methods for exosome isolation and analysis, Cells 8 (2019), https://doi.org/10.3390/cells8070727.

[34] G. Bodega, M. Alique, L. Puebla, J. Carracedo, R.M. Ramirez, Microvesicles: ROS scavengers and ROS producers, J. Extracell. Vesicles 8 (2019) 1626654, https://doi.org/10.1080/20013078.2019.1626654. D.O.I:.

[35] D. Burger, M. Turner, M.N. Munkonda, R.M. Touyz, Endothelial microparticle-derived reactive oxygen species: role in endothelial signaling and vascular function, Oxid. Med. Cell. Longev. (2016) 5047954, https://doi.org/10.1155/2016/5047954, 2016.

[36] N. Javeed, et al., Immunosuppressive CD14(+)HLA-DR(lo/neg) monocytes are elevated in pancreatic cancer and "primed" by tumor-derived exosomes, OncoImmunology 6 (2017) e1252013, https://doi.org/10.1080/2162402X.2016.1252013.

[37] H. Zhang, et al., CD4(+) T cell-released exosomes inhibit CD8(+) cytotoxic T-lymphocyte responses and antitumor immunity, Cell. Mol. Immunol. 8 (2011) 23–30, https://doi.org/10.1038/cmi.2010.59. D.O.I:.

[38] W. Kolowos, et al., Microparticles shed from different antigen-presenting cells display an individual pattern of surface molecules and a distinct potential of allogeneic T-cell activation, Scand. J. Immunol. 61 (2005) 226–233, https://doi.org/10.1111/j.1365-3083.2005.01551.x. D.O.I:.

[39] E. Sum, et al., The tumor-targeted CD40 agonist CEA-CD40 promotes T cell priming via a dual mode of action by increasing antigen delivery to dendritic cells and enhancing their activation, J Immunother Cancer 10 (2022), https://doi.org/10.1136/jitc-2021-003264.

[40] A. Trostchansky, R. Moore-Carrasco, E. Fuentes, Oxidative pathways of arachidonic acid as targets for regulation of platelet activation, Prostag. Other Lipid Mediat. 145 (2019) 106382, https://doi.org/10.1016/j.prostaglandins.2019.106382. D.O.I:.

[41] F. Puhm, E. Boilard, K.R. Machlus, Platelet extracellular vesicles: beyond the blood, Arterioscler. Thromb. Vasc. Biol. 41 (2021) 87–96, https://doi.org/10.1161/ATVBAHA.120.314644. D.O.I:.

[42] X. Osteikoetxea, et al., Improved characterization of EV preparations based on protein to lipid ratio and lipid properties, PLoS One 10 (2015) e0121184, https://doi.org/10.1371/journal.pone.0121184. D.O.I:.

[43] M. Holopainen, et al., Polyunsaturated fatty acids modify the extracellular vesicle membranes and increase the production of proresolving lipid mediators of human mesenchymal stromal cells, Biochim. Biophys. Acta Mol. Cell Biol. Lipids 1864 (2019) 1350–1362, https://doi.org/10.1016/j.bbalip.2019.06.010. D.O.I:.

[44] S. Papadopoulos, et al., Secretory phospholipase A(2)-IIA protein and mRNA pools in extracellular vesicles of bronchoalveolar lavage fluid from patients with early acute respiratory distress syndrome: a new perception in the dissemination of inflammation? Pharmaceuticals 13 (2020) https://doi.org/10.3390/ph13110415.

[45] A.E. Berezin, A.A. Berezin, Extracellular vesicles and thrombogenicity in atrial fibrillation, Int J Mol Sci 23 (2022), https://doi.org/10.3390/ijms23031774.

[46] E.I. Sinauridze, et al., Platelet microparticle membranes have 50- to 100-fold higher specific procoagulant activity than activated platelets, Thromb Haemost 97 (2007) 425–434. D.O.I:.

[47] D. Castano, L.F. Garcia, M. Rojas, Increased frequency and cell death of CD16+ monocytes with Mycobacterium tuberculosis infection, Tuberculosis 91 (2011) 348–360, https://doi.org/10.1016/j.tube.2011.04.002. D.O.I:.

[48] M. Syedbasha, et al., Interferon-lambda enhances the differentiation of naive B cells into plasmablasts via the mTORC1 pathway, Cell Rep. 33 (2020) 108211, https://doi.org/10.1016/j.celrep.2020.108211. D.O.I:.

[49] C. Burbano, et al., HMGB1(+) microparticles present in urine are hallmarks of nephritis in patients with systemic lupus erythematosus, Eur. J. Immunol. 49 (2019) 323–335, https://doi.org/10.1002/eji.201847747. D.O.I:.

[50] C. Burbano, et al., Extracellular vesicles are associated with the systemic inflammation of patients with seropositive rheumatoid arthritis, Sci. Rep. 8 (2018) 17917, https://doi.org/10.1038/s41598-018-36335-x. D.O.I:.

[51] D.B. Kuhns, D.A.L. Priel, J. Chu, K.A. Zarember, Isolation and functional analysis of human neutrophils, Curr. Protoc. Im. 111 (2015), https://doi.org/10.1002/0471142735.im0723s111, 7 23 21-27 23 16. D.O.I:.

[52] J. Hu, et al., Increased neutrophil respiratory burst predicts the risk of coronary artery lesion in kawasaki disease, Front Pediatr 8 (2020) 391, https://doi.org/10.3389/fped.2020.00391. D.O.I:.

[53] E.G. Bligh, W.J. Dyer, A rapid method of total lipid extraction and purification, Can. J. Biochem. Physiol. 37 (1959) 911–917, https://doi.org/10.1139/o59-099. D.O.I:.

[54] W.R. Morrison, L.M. Smith, Preparation of fatty acid methyl esters and dimethylacetals from lipids with boron fluoride–methanol, J. Lipid Res. 5 (1964) 600–608. D.O.I:.

[55] National Research Council (US) Committee on Guidelines for the Use of Animals in Neuroscience and Behavioral Research, Guidelines for the care and use of mammals in neuroscience and behavioral research., Wash. Times: A, Sample Size Determination, National Academies Press, (US), 2003, pp. 175–181, 1.

[56] M. Covington, et al., Preclinical characterization of itacitinib (INCB039110), a novel selective inhibitor of JAK1, for the treatment of inflammatory diseases, Eur. J. Pharmacol. 885 (2020) 173505, https://doi.org/10.1016/j.ejphar.2020.173505. D.O.I:.

[57] V. Gurbuz, et al., Effects of AG490 and S3I-201 on regulation of the JAK/STAT3 signaling pathway in relation to angiogenesis in TRAIL-resistant prostate cancer cells in vitro, Oncol. Lett. 7 (2014) 755–763, https://doi.org/10.3892/ol.2014.1795. D.O.I:.

[58] S. Kubo, et al., Janus kinase inhibitor baricitinib modulates human innate and adaptive immune system, Front. Immunol. 9 (2018) 1510, https://doi.org/10.3389/fimmu.2018.01510. D.O.I:.

[59] B. Verstockt, M. Ferrante, S. Vermeire, G. Van Assche, New treatment options for inflammatory bowel diseases, J. Gastroenterol. 53 (2018) 585–590, https://doi.org/10.1007/s00535-018-1449-z. D.O.I:.

[60] S. Banerjee, A. Biehl, M. Gadina, S. Hasni, D.M. Schwartz, JAK-STAT signaling as a target for inflammatory and autoimmune diseases: current and future prospects, Drugs 77 (2017) 521–546, https://doi.org/10.1007/s40265-017-0701-9. D.O.I:.

[61] P. Mease, et al., Incidence of venous and arterial thromboembolic events reported in the tofacitinib rheumatoid arthritis, psoriasis and psoriatic arthritis development programmes and from real-world data, Ann. Rheum. Dis. 79 (2020) 1400–1413, https://doi.org/10.1136/annrheumdis-2019-216761. D.O.I:.

[62] M. Yates, et al., Venous thromboembolism risk with JAK inhibitors: a meta-analysis, Arthritis Rheumatol. 73 (2021) 779–788, https://doi.org/10.1002/art.41580. D.O.I:.

[63] L. Badimon, et al., Microvesicles in atherosclerosis and angiogenesis: from bench to bedside and reverse, Front Cardiovasc Med 4 (2017) 77, https://doi.org/10.3389/fcvm.2017.00077. D.O.I:.

[64] X. Ding, S. Xiang, Endocytosis and human innate immunity, Journal of Immunological Sciences 2 (2018). D.O.I:.

[65] A. Danesh, et al., Granulocyte-derived extracellular vesicles activate monocytes and are associated with mortality in intensive care unit patients, Front. Immunol. 9 (2018) 956, https://doi.org/10.3389/fimmu.2018.00956. D.O.I:.

[66] A.M. Fond, K.S. Ravichandran, Clearance of dying cells by phagocytes: mechanisms and implications for disease pathogenesis, Adv. Exp. Med. Biol. 930 (2016) 25–49, https://doi.org/10.1007/978-3-319-39406-0_2. D.O.I:.

[67] A.A. Tarique, et al., Phenotypic, functional, and plasticity features of classical and alternatively activated human macrophages, Am. J. Respir. Cell Mol. Biol. 53 (2015) 676–688, https://doi.org/10.1165/rcmb.2015-0012OC. D.O.I:.

[68] K. Alvarez, et al., Induction of NF-kappaB inflammatory pathway in monocytes by microparticles from patients with systemic lupus erythematosus, Heliyon 6 (2020) e05815, https://doi.org/10.1016/j.heliyon.2020.e05815.

[69] A.K. Rutman, et al., Immune response to extracellular vesicles from human islets of langerhans in patients with type 1 diabetes, Endocrinology 159 (2018) 3834–3847, https://doi.org/10.1210/en.2018-00649. D.O.I:.

[70] G. Maulucci, et al., Fatty acid-related modulations of membrane fluidity in cells: detection and implications, Free Radic. Res. 50 (2016) S40–S50, https://doi.org/10.1080/10715762.2016.1231403. D.O.I:.

[71] D. Mondal, et al., Modulation of membrane fluidity performed on model phospholipid membrane and live cell membrane: revealing through spatiotemporal approaches of FLIM, FAIM, and TRFS, Anal. Chem. 91 (2019) 4337–4345, https://doi.org/10.1021/acs.analchem.8b04044. D.O.I:.

[72] D. Richard, K. Kefi, U. Barbe, P. Bausero, F. Visioli, Polyunsaturated fatty acids as antioxidants, Pharmacol. Res. 57 (2008) 451–455, https://doi.org/10.1016/j.phrs.2008.05.002. D.O.I:.

[73] H. Fuhrmann, E.A. Miles, A.L. West, P.C. Calder, Membrane fatty acids, oxidative burst and phagocytosis after enrichment of P388D1 monocyte/macrophages with essential 18-carbon fatty acids, Ann. Nutr. Metab. 51 (2007) 155–162, https://doi.org/10.1159/000103276. D.O.I:.

[74] M. Massaro, et al., Quenching of intracellular ROS generation as a mechanism for oleate-induced reduction of endothelial activation and early atherogenesis, Thromb. Haemostasis 88 (2002) 335–344. D.O.I:.
[75] M. Nihad, et al., Arachidonic acid modulates the cellular energetics of human pluripotent stem cells and protects the embryoid bodies from embryotoxicity effects in vitro, Reprod. Toxicol. 120 (2023) 108438, https://doi.org/10.1016/j.reprotox.2023.108438. D.O.I:.
[76] A. Saffaryazdi, A. Ganjeali, R. Farhoosh, M. Cheniany, Variation in phenolic compounds, alpha-linolenic acid and linoleic acid contents and antioxidant activity of purslane (Portulaca oleracea L.) during phenological growth stages, Physiol. Mol. Biol. Plants 26 (2020) 1519–1529, https://doi.org/10.1007/s12298-020-00836-9. D.O.I:.
[77] P. Schonfeld, L. Wojtczak, Fatty acids decrease mitochondrial generation of reactive oxygen species at the reverse electron transport but increase it at the forward transport, Biochim. Biophys. Acta 1767 (2007) 1032–1040, https://doi.org/10.1016/j.bbabio.2007.04.005. D.O.I:.
[78] B. Juttner, et al., Unsaturated long-chain fatty acids induce the respiratory burst of human neutrophils and monocytes in whole blood, Nutr. Metab. 5 (2008) 19, https://doi.org/10.1186/1743-7075-5-19.
[79] R. Soleti, E. Lauret, R. Andriantsitohaina, M. Carmen Martinez, Internalization and induction of antioxidant messages by microvesicles contribute to the antiapoptotic effects on human endothelial cells, Free Radic. Biol. Med. 53 (2012) 2159–2170, https://doi.org/10.1016/j.freeradbiomed.2012.09.021. D.O.I:.
[80] E. Chiaradia, et al., Extracellular vesicles under oxidative stress conditions: biological properties and physiological roles, Cells 10 (2021), https://doi.org/10.3390/cells10071763.
[81] M. Saeed-Zidane, et al., Cellular and exosome mediated molecular defense mechanism in bovine granulosa cells exposed to oxidative stress, PLoS One 12 (2017) e0187569, https://doi.org/10.1371/journal.pone.0187569. D.O.I:.
[82] J.A. Carlsson, A.E. Wold, A.S. Sandberg, S.M. Ostman, The polyunsaturated fatty acids arachidonic acid and docosahexaenoic acid induce mouse dendritic cells maturation but reduce T-cell responses in vitro, PLoS One 10 (2015) e0143741, https://doi.org/10.1371/journal.pone.0143741. D.O.I:.
[83] N.A. Reilly, E. Lutgens, J. Kuiper, B.T. Heijmans, J. Wouter Jukema, Effects of fatty acids on T cell function: role in atherosclerosis, Nat. Rev. Cardiol. 18 (2021) 824–837, https://doi.org/10.1038/s41569-021-00582-9. D.O.I:.
[84] R. Gorjao, M.F. Cury-Boaventura, T.M. de Lima, R. Curi, Regulation of human lymphocyte proliferation by fatty acids, Cell Biochem. Funct. 25 (2007) 305–315, https://doi.org/10.1002/cbf.1388. D.O.I:.
[85] M. Czystowska-Kuzmicz, et al., Small extracellular vesicles containing arginase-1 suppress T-cell responses and promote tumor growth in ovarian carcinoma, Nat. Commun. 10 (2019) 3000, https://doi.org/10.1038/s41467-019-10979-3. D.O.I:.
[86] A.L. Dordevic, N. Konstantopoulos, D. Cameron-Smith, 3T3-L1 preadipocytes exhibit heightened monocyte-chemoattractant protein-1 response to acute fatty acid exposure, PLoS One 9 (2014) e99382, https://doi.org/10.1371/journal.pone.0099382.
[87] H.S. Hwang, et al., Extracellular vesicles as potential therapeutics for inflammatory diseases, Int J Mol Sci 22 (2021), https://doi.org/10.3390/ijms22115487.
[88] R. Fernandez-Botran, Soluble cytokine receptors: basic immunology and clinical applications, Crit. Rev. Clin. Lab Sci. 36 (1999) 165–224, https://doi.org/10.1080/10408369991239196. D.O.I:.
[89] M. Banerjee, S.W. Whiteheart, The ins and outs of endocytic trafficking in platelet functions, Curr. Opin. Hematol. 24 (2017) 467–474, https://doi.org/10.1097/MOH.0000000000000366. D.O.I:.
[90] Z.H. Kwok, C. Wang, Y. Jin, Extracellular vesicle transportation and uptake by recipient cells: a critical process to regulate human diseases, Processes 9 (2021), https://doi.org/10.3390/pr9020273.
[91] A.C. Martin, et al., The effectiveness of platelet supplementation for the reversal of ticagrelor-induced inhibition of platelet aggregation: an in-vitro study, Eur. J. Anaesthesiol. 33 (2016) 361–367, https://doi.org/10.1097/EJA.0000000000000348. D.O.I:.
[92] N. Rukoyatkina, et al., Multifaceted effects of arachidonic acid and interaction with cyclic nucleotides in human platelets, Thromb. Res. 171 (2018) 22–30, https://doi.org/10.1016/j.thromres.2018.09.047. D.O.I:.
[93] H.J. Hong, G.S. Nam, K.S. Nam, Daidzein inhibits human platelet activation by downregulating thromboxane A(2) production and granule release, regardless of COX-1 activity, Int J Mol Sci 24. (2023), https://doi.org/10.3390/ijms241511985.
[94] Y. Li, Q.Y. Li, Q.L. Ling, S.P. So, K.H. Ruan, A novel single-chain enzyme complex with chain reaction properties rapidly producing thromboxane A(2) and exhibiting powerful anti-bleeding functions, J. Cell Mol. Med. 23 (2019) 8343–8354, https://doi.org/10.1111/jcmm.14711. D.O.I:.
[95] J.B. Smith, Prostaglandins and platelet aggregation, Acta Med. Scand. Suppl. 651 (1981) 91–99, https://doi.org/10.1111/j.0954-6820.1981.tb03638.x. D.O.I:.
[96] P. Mehta, J. Mehta, D. Lawson, I. Krop, L.G. Letts, Leukotrienes potentiate the effects of epinephrine and thrombin on human platelet aggregation, Thromb. Res. 41 (1986) 731–738, https://doi.org/10.1016/0049-3848(86)90370-1. D.O.I:.
[97] A.J. Bertolin, et al., Platelet reactivity and coagulation markers in patients with COVID-19, Adv. Ther. 38 (2021) 3911–3923, https://doi.org/10.1007/s12325-021-01803-w. D.O.I:.